An Analysis of Polarization Phenomena for Sensing Applications

Ana Mendes Teixeira
Master in Engineering Physics
Department of Physics and Astronomy
Faculty of Sciences of University of Porto and Faculty of Engineering of University of Porto
2025

U.PORTO
FACULDADE DE CIÊNCIAS
UNIVERSIDADE DO PORTO

U.PORTO
FEUP FACULDADE DE ENGENHARIA
UNIVERSIDADE DO PORTO

MSC

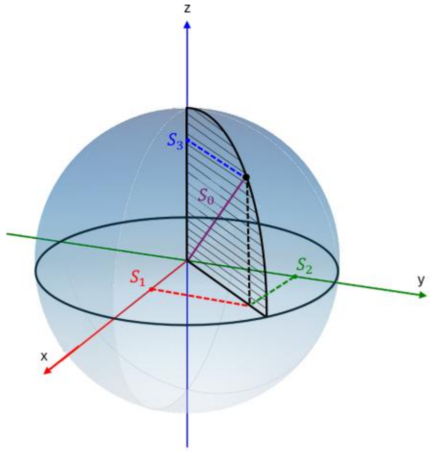

An Analysis of Polarization Phenomena for Sensing Applications

Ana Mendes Teixeira
Dissertation carried out as part of the Master in Engineering Physics
Department of Physics and Astronomy
2025

Supervisor
Dr. Susana Silva, Assistant Researcher, INESC TEC

Co-supervisor
Dr. Orlando Frazão, Area Manager, INESC TEC

INESCTEC
ASSOCIATE LABORATORY
PORTUGAL

“ If every porkshop was perfect we wouldn’t have hot dogs. ”

Steven Universe, Greg

Acknowledgements

Firstly, I would like to thank my supervisors, Susana Silva and Orlando Frazão, not only for guiding me throughout this dissertation, and introducing me to the world of scientific research, as well as for always having my best interest in mind. Thank you for all the words of encouragement, and for always finding the time to oversee my progress. Thank you for making me part of the team, but especially for making me feel part of it. To this team, thank you for all the ideas shared and for the help in the lab.

To my parents, who have always supported my goals and dreams. Thank you for believing in me and for all your support. To my mother, who was always there to talk and to comfort me when I was worried. To my father, for making learning fun with games and challenges. Thank you both for teaching me that anything is possible with enough dedication.

To my sister, who is the most annoying person I know. Thank you for making me want to be better, to give you a good example and to set the expectations high. Thank you for all the conversations, jokes and games.

To my friends, who have been there for me in this academic journey. Thank you for all the incredible nights out, and for all the study sessions that you made bright, thank you for everything. Thank you for the climbing sessions, the coffees after lunch, and all the laughs that we share. To the ones in black, a special thanks for making me a better person and for making college feel like home.

Finally, this dissertation would not be possible without Tiago. Thank you for all the encouragement and all the love you give every day. For all the discussions and for always trying to help me in everything. Thank you for believing in me and making me believe in myself. Thank you for always being by my side.

Resumo

A rede global de cabos submarinos de telecomunicações representa uma vasta infraestrutura potencial para monitorização sísmica e ambiental distribuída. A deteção polarimétrica, que analisa alterações coerentes no estado de polarização (SOP) da luz, surgiu como uma técnica poderosa para este fim. No entanto, a sua implementação prática enfrenta desafios significativos, nomeadamente as incertezas dependentes da polarização e a necessidade de caracterizar totalmente a resposta do sensor a parametros físicos essenciais.

Esta dissertação aborda esses desafios por meio de uma investigação abrangente dividida em três fases principais. A investigação começa com uma caracterização experimental de um amplificador de fibra dopada com érbio (EDFA) comercial, quantificando o seu ganho dependente da polarização (PDG) e, crucialmente, o seu impacto na estabilidade de fase do sinal ótico. Esta análise é alargada a uma configuração de longas distâncias com 50 km de fibra, revelando um desvio de fase significativo que representa um desafio para medições polarimétricas sensíveis.

Em seguida, um sensor polarimétrico é implementado usando um polarímetro comercial para medir os parâmetros de Stokes. A resposta do sistema à temperatura, tensão axial e torção da fibra é caracterizada experimentalmente, demonstrando sua capacidade de detecção multiparamétrica com precisão satisfatória.

Por fim, para aumentar a sensibilidade, é implementado um 'fiber loop mirror' (FLM) de alta birrefringência. Esta configuração aumenta a sensibilidade à deformação em uma ordem de magnitude quando os parametros iniciais certos. Além disso, a montagem FLM é adaptada para criar um sensor de rotação polarimétrico de protótipo, demonstrando uma resposta clara às mudanças angulares com uma resolução de 1°.

Os resultados concluem que, embora os amplificadores óticos introduzam polarização e ruído de fase, a deteção polarimétrica é uma técnica altamente viável. O aumento de sensibilidade demonstrado através de um FLM e a medição bem sucedida de parâmetros físicos essenciais reforçam fortemente o potencial desta tecnologia para aplicações avançadas, como a deteção sísmica distribuída em redes de cabos submarinos.

Palavras-chave: Física, ótica, sensor em fibra, polarização, EDFA, parametros de Stokes, polarímetro, 'fiber loop mirror'

Abstract

The global network of submarine telecommunication cables is an infrastructure with a vast potential for distributed seismic and environmental monitoring. Polarimetric sensing, which analyzes coherent changes in the state of polarization (SOP) of light, has emerged as a powerful technique for this purpose. However, its practical implementation faces significant challenges, notably the polarization-dependent impairments and the need to fully characterize the sensor's response to key physical parameters.

This dissertation addresses these challenges through a comprehensive investigation divided into three core phases. The research begins with an experimental characterization of a commercial Erbium-Doped Fiber Amplifier (EDFA), quantifying its Polarization-Dependent Gain (PDG) and, crucially, its impact on the phase stability of the optical signal. This analysis is extended to a long-haul configuration with 50 km of fiber, revealing significant phase drift that poses a challenge for sensitive polarimetric measurements.

A simple polarimetric sensor is then implemented using a commercial polarimeter to measure Stokes parameters. The system's response to temperature, axial strain, and fiber twist is experimentally characterized, demonstrating its capability for multi-parameter sensing with satisfactory accuracy.

Finally, to enhance sensitivity, a high-birefringence Fiber Loop Mirror (FLM) is implemented. This configuration successfully increases the strain sensitivity by an order of magnitude for an optimal initial state of polarization. Furthermore, the FLM architecture is adapted to create a proof-of-concept polarimetric rotation sensor, demonstrating a clear response to angular changes with a resolution of 1°.

The findings conclude that while optical amplifiers introduce polarization and phase noise, polarimetric sensing is a highly viable technique. The demonstrated sensitivity enhancement via an FLM and the successful measurement of key physical parameters strongly support the potential of this technology for advanced applications like distributed seismic sensing on submarine cable networks.

Keywords: physics, optics, fiber sensing, polarization, EDFA, Stokes parameters, polarimeter, fiber loop mirror

Table of Contents

List of Tables

List of Figures

List of Abbreviations

ASE Amplified Spontaneous Emission

DAS Distributed Acoustic Sensing

DFOS Distributed Optical Fiber Sensor

EDFA Erbium-Doped Fiber Amplifier

EMI Electromagnetic Interference

FBG Fiber Bragg Grating

FLM Fiber Loop Mirror

FOG Fiber-Optic-Gyroscope

FSK Frequency-Shift-Keying

HI-BI High-Birrefringence

HLPG Helical Long-Period Fiber Grating

L+45 Linear $+45°$ Polarization

L-45 Linear $-45°$ Polarization

LCP Left Circular Polarization

LHP Linear Horizontal Polarization

LPFG Long-Period Fiber Grating

LVP Linear Vertical Polarization

MEMS Micro-Electro-Mechanical Systems

OSA Optical Spectrum Analyzer

PDG Polarization Dependent Gain

PMD Polarization Mode Dispersion

RCP Right Circular Polarization

RTD Resistance Temperature Detector

SOP State of Polarization

1. Introduction

1.1. Motivation

The detection and monitoring of seismic activity are fundamental to understanding tectonic processes, assessing geological hazards, and implementing effective early warning systems. However, traditional seismic networks, which rely on sparsely distributed land-based seismometers, leave over two-thirds of the Earth's surface—the oceans—as a vast blind spot. The deployment and maintenance of permanent seafloor observatories are technologically complex and prohibitively expensive, creating a critical gap in our global geophysical monitoring capabilities.

A paradigm shift emerged with the demonstration that existing submarine telecommunication cables could be repurposed as continuous, distributed seismic sensors. Among the various sensing techniques, polarimetric sensing has proven to be a particularly powerful method. By analyzing coherent changes in the State of Polarization (SOP) of light propagating through a fiber-optic cable, it is possible to detect minute strain and temperature perturbations caused by seismic and ocean waves. This approach leverages the inherent birefringence of the optical fiber, which acts as a distributed transducer of mechanical stress, converting it into a measurable modulation of the light's polarization.

Despite its promise, the practical implementation of this technique faces significant challenges. The transmission of a stable, measurable optical signal over transoceanic distances requires in-line amplification via Erbium-Doped Fiber Amplifiers (EDFAs). A key impediment is that EDFAs themselves introduce polarization-dependent impairments, most notably Polarization-Dependent Gain (PDG) and additional phase noise, which can distort the SOP and obscure the environmental signals the system aims to detect. Furthermore, accurately interpreting the SOP data to distinguish seismic signals from other noise requires a fundamental understanding of the sensor's response to basic physical parameters like strain, temperature, and torsion in a controlled environment.

This dissertation is motivated by the need to address these foundational challenges and advance the technology of polarimetric sensing. The work done is driven by the goal of contributing to the development of robust and reliable systems that can transform the global network of submarine cables into a powerful tool for Earth science and hazard mitigation.

1.2. Aim and Objectives

The overarching aim of this dissertation is to investigate polarization effects in optical fiber systems, both as a source of impairment in amplified communication links and as a sensing mechanism for physical parameters, with a view towards applications in seismic detection.

To achieve this aim, the following specific objectives were defined:

1. To characterize the polarization-dependent properties of a commercial Erbium-Doped Fiber Amplifier (EDFA). This involves measuring its Polarization-Dependent Gain (PDG) and, crucially, analyzing its impact on the phase of the optical signal under various operating conditions.
2. To design and implement a polarimetric sensor based on the measurement of Stokes parameters using a commercial polarimeter.
3. To experimentally demonstrate and quantify the sensitivity of the polarimetric sensor to key physical parameters relevant to seismic sensing, namely temperature, axial strain, and fiber twist.
4. To explore methods for enhancing sensor sensitivity by implementing a fiber loop mirror (FLM) interferometer and evaluating its performance compared to a simple transmission-based setup.
5. To synthesize the findings from the characterization and sensing experiments to discuss the implications for real-world applications, particularly distributed seismic sensing using submarine cables.

1.3. Structure of the dissertation

This dissertation is structured into five chapters, including this introduction.

Chapter 2: Polarization concepts and state-of-the-art. This chapter provides the necessary theoretical foundation for the thesis. It begins with a description of the polarization of light, introducing the Stokes parameters and their representation on the Poincaré sphere.

This is followed by a historical overview of polarimetric optical fiber sensors, culminating in a review of the current state-of-the-art in polarization-based seismic sensing using submarine telecommunication cables.

Chapter 3: Study of polarization effects in Erbium-Doped Fiber Amplifiers. This chapter presents an experimental characterization of a commercial EDFA. The amplifier's gain saturation is first evaluated. Subsequently, a detailed analysis of the evolution of the Stokes parameters and optical phase is conducted for different input power levels and in a long-haul configuration with 50 km of fiber, quantifying the polarization-dependent gain and phase instability.

Chapter 4: Measure of physical parameters using a polarimeter. This chapter demonstrates the application of a polarimetric setup for sensing. The system's response to temperature changes, fiber twist, and axial strain is experimentally characterized.

Chapter 5: Study of a Fiber Loop Mirror setup to enhance the sensitivity of the polarimetric strain sensor. Moreover, the method implemented to the strain sensor is used to develop a functional rotation sensor.

Chapter 6: Discussion and Conclusion. This final chapter synthesizes the main findings of the thesis. It discusses the results from the EDFA characterization in the context of long-haul sensing systems and evaluates the performance of the polarimetric sensor. The chapter concludes by summarizing the key contributions of the work and proposing directions for future research.

1.4. Outputs

A Teixeira, J Tavares, J Araújo, HM Salgado, S Silva, O Frazão, "The effect of amplification on the state of polarization over 50 km using an EDFA," EOSAM 2025 Conference, EPJ Web of Conferences 335, 03047 (2025) – Poster presentation.

Ana Teixeira, Susana Silva, Orlando Frazão, "Sensing fiber twist through state of polarization-induced phase shifts," RIAO-OPTILAS 2025 Conference, Universidad Privada Boliviana in Bolivia, November 17 to 21, 2025 – Oral presentation.

2. Polarization concepts and state-of-the-art

Polarimetric sensors are based on polarimetry, which is the measurement of all polarization properties of a light beam (Stokes polarimetry) or a material interacting with a light beam (Mueller polarimetry). The use of polarization in sensors provides a richer set of information compared to traditional imaging methods, enabling improved detection, identification, and analysis in a wide range of applications. These advantages make polarimetric sensors an invaluable tool.

While polarimeters have diverse applications in both free-space and fiber optics, the present study will concentrate on polarimetric sensors within optical fibers. The operation of these sensors is based on the detection of perturbations in the medium surrounding the fiber.

In this chapter, the basic working principles of the polarization of light and polarimetric sensors is presented, followed by a historical overview of the study of polarization and the application of polarimetric optical fiber sensors.

2.1. Polarization of Light

Light's polarization is a manifestation of its fundamental vectorial nature, defined by the orientation of its oscillating electric field. Unlike longitudinal waves (like sound), where oscillations occur parallel to the direction of travel, light's electric and magnetic field components oscillate in directions perpendicular to each other and to the wave's direction of propagation. This means that light is a transverse wave (Fig. 2.1), which entails that the electric field can be resolved into two independent, orthogonal components that can define the state of polarization. Understanding this vectorial description is essential for polarimetry, as any interaction of light with a material—such as a fiber—can alter this relationship, providing a measurable signal of the perturbation.

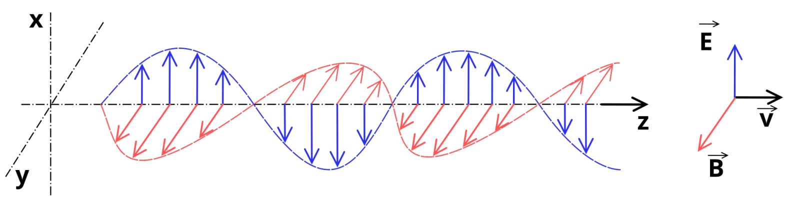

FIGURE 2.1: Electromagnetic wave propagating along the positive z-axis, showing the electric field (blue) and magnetic field (red) vectors [1].

The polarization behavior can be represented in terms of observables, that are called Stokes parameters. There are four parameters, which are obtained by doing the time average of the unobserved polarization ellipse. Together, these parameters give a complete description of any polarization state of light [2].

2.1.1 The Stokes Polarization Parameters

In 1852 Sir George Gabriel Stokes discovered that the polarization behavior can be represented in terms of observables, the Stokes parameters.

Originally, the Stokes parameters were used only to describe the measured intensity and polarization state of the optical field. But by forming the Stokes parameters in terms of a column matrix, the so-called Stokes vector, we are led to a formulation in which we obtain not only measurables but also observables, which can be seen in a spectroscope.

In order to derive the Stokes parameters, as was said before, light needs to be considered as two transverse waves that can be represented by equations 2.1 and 2.2, where z is the direction of propagation of light, t is time, $E_{0x}(t)$ and $E_{0y}(t)$ are the instantaneous amplitudes, ω is the instantaneous angular frequency, and $\delta_x(t)$ and $\delta_y(t)$ are the instantaneous phase factors:

$$E_x(z,t) = E_{0x}(t)\cos[\omega t + \delta_x(t)] \tag{2.1}$$

$$E_y(z,t) = E_{0y}(t)\cos[\omega t + \delta_y(t)] \tag{2.2}$$

Through simple manipulation of the terms in Eqs. 2.1 and 2.2, and by explicitly eliminating the ωt term, the familiar expression for an ellipse (Eq. 2.3), known as the polarization ellipse, is obtained, where $\Delta\delta = \delta_y - \delta_x$. The expression is simplified by considering monochromatic radiation, where the amplitudes and phases are constant in time.

$$\frac{E_x^2(t)}{E_{0x}^2} + \frac{E_y^2(t)}{E_{0y}^2} - \frac{2E_x(t)E_y(t)}{E_{0x}E_{0y}}\cos\Delta\delta = \sin^2\Delta\delta \tag{2.3}$$

The representation of the Polarization Ellipse is shown in Fig. 2.2, where ψ is the orientation angle (Eq. 2.9).

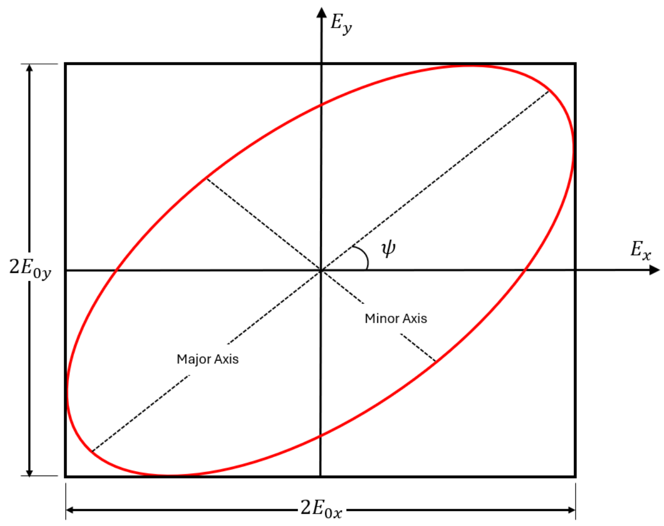

FIGURE 2.2: The Polarization Ellipse representation of polarized light.

To obtain the Stokes parameters, which are observables, an average over a period of oscillation must be applied to Eq. 2.3, obtaining Eq. 2.4 after some manipulation.

$$\left(E_{0x}^2 + E_{0y}^2\right)^2 = \left(E_{0x}^2 - E_{0y}^2\right)^2 + \left(2E_{0x}E_{0y}\cos\Delta\delta\right)^2 + \left(2E_{0x}E_{0y}\sin\Delta\delta\right)^2 \tag{2.4}$$

The quantities in parentheses are the Stokes parameters:

$$\begin{aligned} S_0 &= E_{0x}^2 + E_{0y}^2 \\ S_1 &= E_{0x}^2 - E_{0y}^2 \\ S_2 &= 2E_{0x}E_{0y}\cos\Delta\delta \\ S_3 &= 2E_{0x}E_{0y}\sin\Delta\delta \end{aligned} \tag{2.5}$$

The first Stokes parameter S_0 is the total intensity of the light. The parameter S_1 describes the amount of linear horizontal or vertical polarization, the parameter S_2 describes the amount of linear $+45°$ or $-45°$ polarization, and the parameter S_3 describes the amount of right or left circular polarization contained within the beam.

The Stokes parameters for any state of polarization obey the relation presented in Eq. 2.6. This relation becomes an equality in the case of completely polarized light, and an inequality for partially polarized or unpolarized light*.

*Unpolarized light, being unaffected by an analyzer or retarder, is characterized by $S_1 = S_2 = S_3 = 0$.

$$S_0^2 \geq S_1^2 + S_2^2 + S_3^2 \tag{2.6}$$

The Stokes parameters allow one to define the degree of polarization (DOP), which quantifies the fraction of total light intensity that is polarized. It ranges from 0 (unpolarized) to 1 (completely polarized) as given by (2.7). In this definition, the total intensity I_{tot} is given by the parameter S_0, while the intensity I_{pol} of the polarized component is derived from the parameters S_1, S_2, and S_3 that describe the polarization state.

$$DOP = \frac{I_{pol}}{I_{tot}} = \frac{\sqrt{S_1^2 + S_2^2 + S_3^2}}{S_0} \tag{2.7}$$

The Stokes parameters can also be represented in the form of a matrix, called the Stokes vector. Mathematically, it is not a vector, but, customarily, it is called a vector.

$$S = \begin{pmatrix} S_0 \\ S_1 \\ S_2 \\ S_3 \end{pmatrix} = S_0 \begin{pmatrix} 1 \\ \cos 2\chi \cos 2\psi \\ \cos 2\chi \sin 2\psi \\ \sin 2\chi \end{pmatrix} = I_0 \begin{pmatrix} 1 \\ \cos 2\alpha \\ \sin 2\alpha \cos \Delta\delta \\ \sin 2\alpha \sin \Delta\delta \end{pmatrix} \tag{2.8}$$

The general expression for the Stokes vector is shown in Eq. 2.8, where ψ is the orientation angle (Eq. 2.9) and χ is the ellipticity angle (Eq. 2.10).

$$\tan 2\psi = \frac{S_2}{S_1} = \tan 2\alpha \cos \Delta\delta \tag{2.9}$$

$$\sin 2\chi = \frac{S_3}{S_0} = \sin 2\alpha \sin \Delta\delta \tag{2.10}$$

These quantities define important characteristics of the polarization of light, namely the orientation angle of the polarization ellipse and its ellipticity.

Another important quantity used throughout this dissertation is the phase of light, $\Delta\delta$. Its relationship to the Stokes parameters is established through the components S_2 and S_3 from Eq. 2.8: $S_2 = \sin 2\alpha \cos \Delta\delta$ and $S_3 = \sin 2\alpha \sin \Delta\delta$. From these relations, the phase is defined by Eq. 2.11 [3].

$$\Delta\delta = \arctan\left(\frac{S_3}{S_2}\right) \tag{2.11}$$

2.1.2 The Poincaré Sphere

Although the Stokes parameters offer a complete mathematical characterization of polarization, they lack an intuitive visual representation. Consequently, the polarization ellipse is often employed as a graphical tool. However, this representation has several limitations. As a beam of light travels through space, the light vector traces out an ellipse in a plane perpendicular to the direction of propagation. This occurs over an extremely short time interval, on the order of 10^{-15} seconds. Such a brief timescale makes it impossible to observe the actual tracing of the ellipse in real time, effectively preventing us from directly observing the polarization ellipse. Additionally, the concept of the polarization ellipse is only suitable for describing fully polarized light. It cannot be applied to unpolarized or partially polarized light, further restricting its usefulness.

Around 1890, Henri Poincaré discovered that the polarization ellipse could be represented on a complex plane and projected onto a sphere using stereographic projection. This sphere, later known as the Poincaré sphere, is extremely valuable for visualizing polarized light, especially for describing the change in polarized light when it interacts with polarizing elements. Poincaré introduced this concept in his 1892 work, *Théorie Mathemátique de la Lumière* [4].

One of the most useful features of the Poincaré sphere is that each point on the sphere represents the three Stokes parameters for elliptically polarized light. Additionally, the degree of interaction between a polarized beam and an optical polarizing element is represented by a rotation of the sphere.

It is pretty easy to understand how the Stokes vector can be represented in a sphere. Recalling Eq. 2.8, the Stokes parameters S_1, S_2 and S_3 are almost identical in form to the well-known equations relating Cartesian coordinates to spherical coordinates:

$$\begin{aligned} x &= r\sin\theta\cos\phi \\ y &= r\sin\theta\sin\phi \\ z &= r\cos\theta \end{aligned} \tag{2.12}$$

Comparing the expressions 2.8 and 2.12 it is concluded that $\theta = 90° - 2\chi$ and $\phi = 2\psi$ in Eq. 2.12. The state of polarization (SOP) can be described by the parameters χ and ψ, which describe its ellipticity and orientation, respectively. When plotted on a sphere of unit radius $(S_0 = 1)$, these parameters provide a complete geometric representation. The conventional form of this sphere, the Poincaré sphere, is illustrated in Fig. 2.3.

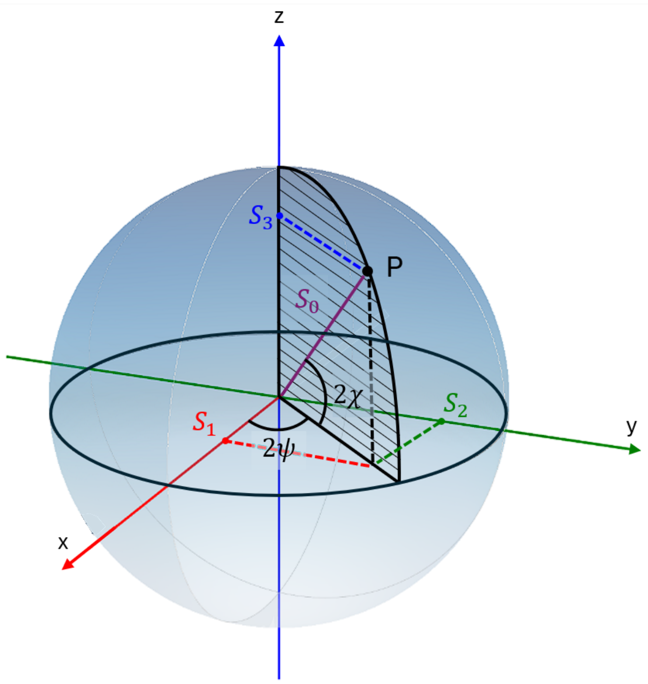

FIGURE 2.3: The Poincaré sphere representation of polarized light.

In this representation, the interior of the sphere $(S_0 < 1)$ represents partially polarized light, while the surface $(S_0 = 1)$ corresponds to fully polarized light. Moreover, for fully polarized light, the equator indicates linear polarization $(S_3 = 0)$, the poles represent circular polarization $(S_1 = S_2 = 0)$, and all other points denote elliptical polarization.

Several notable cases of polarized light (Fig. 2.4) will be presented. Although some cases may seem redundant due to their similarities, understanding each one is essential for unambiguous identification.

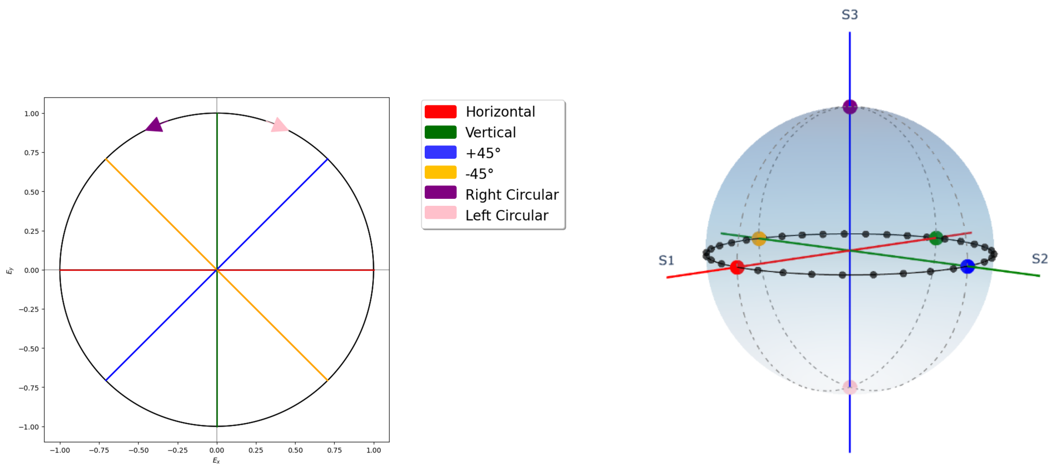

(A) Polarization Ellipse

(B) Poincare Sphere

FIGURE 2.4: Notable cases of polarized light. (A) Polarization Ellipse. (B) Poincaré Sphere.

2.1.2.1 Linear Horizontally Polarized Light (LHP)

In the case of linear horizontally polarized light, $E_{0y} = 0$. Recalling Eq. 2.5 and assuming $I_0 = S_0 = E_{0x}^2$, one obtains the Stokes vector as follows:

$$S = \begin{pmatrix} E_{0x}^2 \\ E_{0x}^2 \\ 0 \\ 0 \end{pmatrix} = I_0 \begin{pmatrix} 1 \\ 1 \\ 0 \\ 0 \end{pmatrix} \tag{2.13}$$

Figure 2.5 presents (A) the Polarization Ellipse and (B) the Poincaré Sphere of the LHP state.

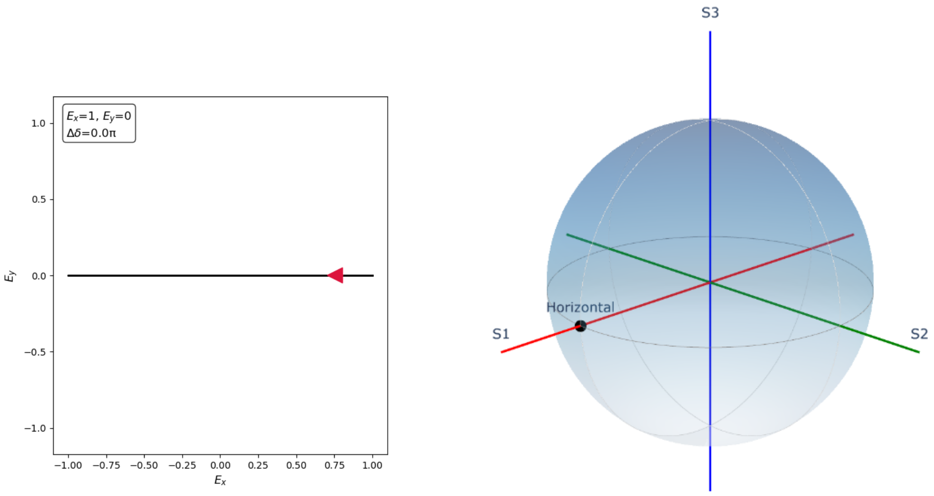

(A) Poincaré Sphere. (B) Polarization Ellipse.

FIGURE 2.5: Linear horizontal polarization state. (A) Polarization Ellipse. (B) Poincaré Sphere.

2.1.2.2 Linear Vertically Polarized Light (LVP)

In the case of linear vertically polarized light, $E_{0x} = 0$, considering $I_0 = S_0 = E_{0y}^2$, the Stokes vector gets the form:

$$S = \begin{pmatrix} E_{0y}^2 \\ -E_{0y}^2 \\ 0 \\ 0 \end{pmatrix} = I_0 \begin{pmatrix} 1 \\ -1 \\ 0 \\ 0 \end{pmatrix} \tag{2.14}$$

Figure 2.6 presents (A) the Polarization Ellipse and (B) the Poincaré Sphere of the LVP state.

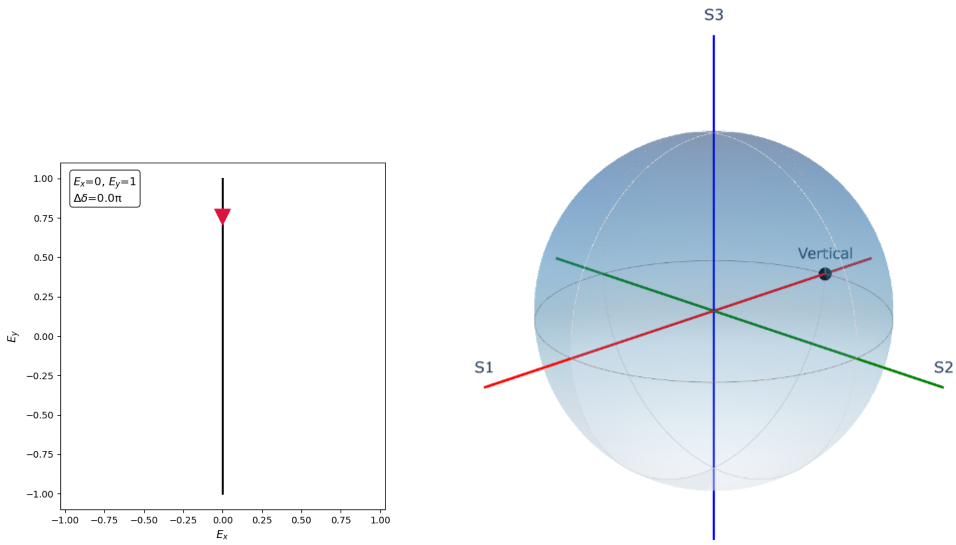

(A) Polarization Ellipse (B) Poincare Sphere

FIGURE 2.6: Linear vertical polarization state. (A) Polarization Ellipse. (B) Poincaré Sphere.

2.1.2.3 Linear +45° Polarized Light (L+45)

When linear polarized light rotates $+45°$ (L+45), $E_{0x} = E_{0y} = E_0$ and $\Delta\delta = 0°$. Considering $I_0 = S_0 = 2E_0^2$ the Stokes vector becomes as follows:

$$S = \begin{pmatrix} 2E_0^2 \\ 0 \\ 2E_0^2 \\ 0 \end{pmatrix} = I_0 \begin{pmatrix} 1 \\ 0 \\ 1 \\ 0 \end{pmatrix} \tag{2.15}$$

Figure 2.7 presents (A) the Polarization Ellipse and (B) the Poincaré Sphere of the L+45 polarization state.

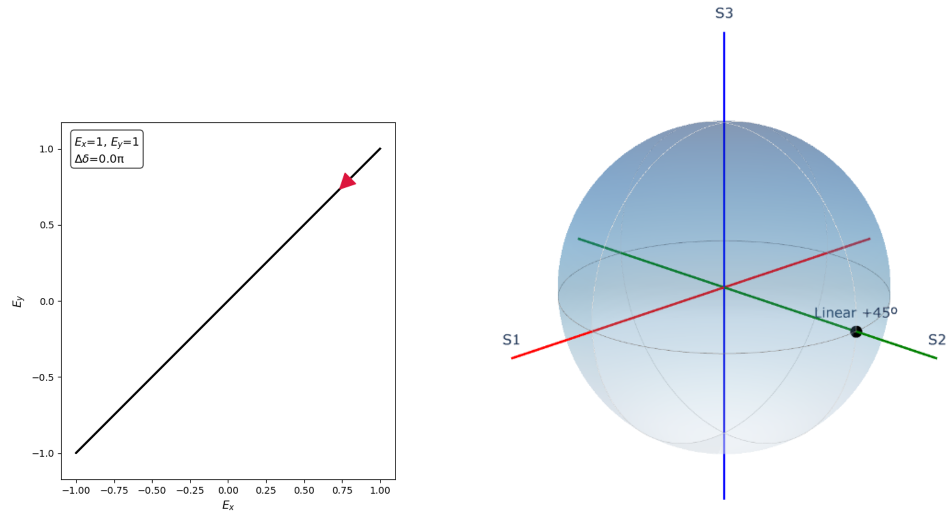

(A) Polarization Ellipse (B) Poincare Sphere

FIGURE 2.7: Linear +45º polarization state.(A) Polarization Ellipse. (B) Poincaré Sphere.

2.1.2.4 Linear -45° Polarized Light (L-45)

When linear polarized light rotates $-45°$ (L+45), $E_{0x} = E_{0y} = E_0$ and $I_0 = S_0 = 2E_0^2$. However, $\Delta\delta = 180°$ thus leading to the following Stokes vector:

$$S = \begin{pmatrix} 2E_0^2 \\ 0 \\ -2E_0^2 \\ 0 \end{pmatrix} = I_0 \begin{pmatrix} 1 \\ 0 \\ -1 \\ 0 \end{pmatrix} \tag{2.16}$$

Figure 2.8 shows (A) the Polarization Ellipse and (B) the Poincaré Sphere of the L-45 polarization state.

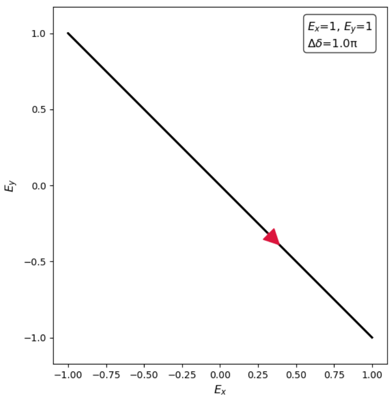

(A) Polarization Ellipse

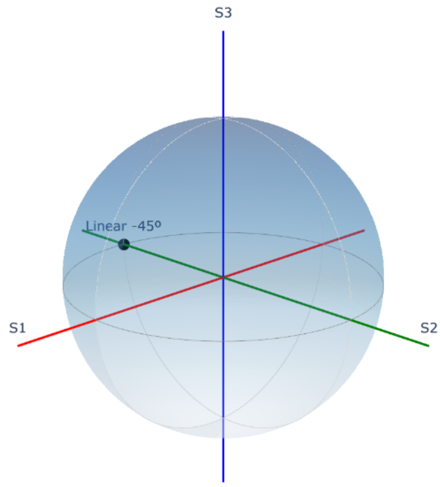

(B) Poincare Sphere

FIGURE 2.8: Linear -45º polarization state.(A) Polarization Ellipse. (B) Poincaré Sphere.

2.1.2.5 Right Circularly Polarized Light (RCP)

In the case of right circularly polarized (RCP) light, $E_{0x} = E_{0y} = E_0$ and $\Delta\delta = 90°$. Considering $I_0 = S_0 = 2E_0^2$, the Stokes vector becomes as follows:

$$S = \begin{pmatrix} 2E_0^2 \\ 0 \\ 0 \\ 2E_0^2 \end{pmatrix} = I_0 \begin{pmatrix} 1 \\ 0 \\ 0 \\ 1 \end{pmatrix} \tag{2.17}$$

Figure 2.9 shows (A) the Polarization Ellipse and (B) the Poincaré Sphere of the RCP state.

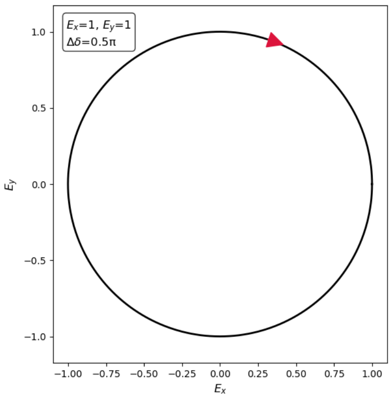

(A) Polarization Ellipse

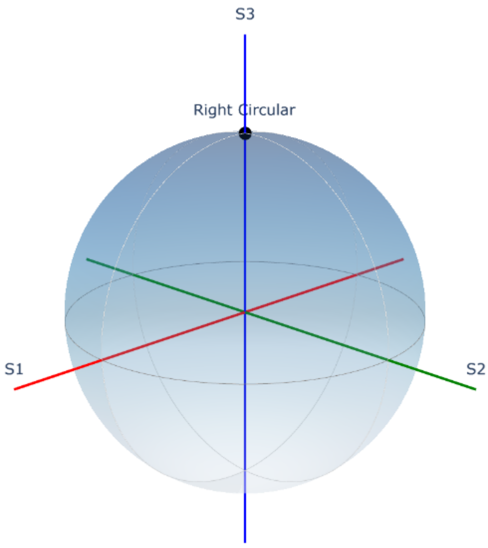

(B) Poincare Sphere

FIGURE 2.9: Circular right polarization state.(A) Polarization Ellipse. (B) Poincaré Sphere.

2.1.2.6 Left Circularly Polarized Light (LCP)

In the case of left circularly polarized (LCP) light, $E_{0x} = E_{0y} = E_0$ and $\Delta\delta = -90°$. Considering $I_0 = S_0 = 2E_0^2$, the Stokes vector gets the form:

For this case $E_{0x} = E_{0y} = E_0$ and $\Delta\delta = -90°$, where $I_0 = S_0 = 2E_0^2$:

$$S = \begin{pmatrix} 2E_0^2 \\ 0 \\ 0 \\ -2E_0^2 \end{pmatrix} = I_0 \begin{pmatrix} 1 \\ 0 \\ 0 \\ -1 \end{pmatrix} \tag{2.18}$$

Figure 2.10 depicts (A) the Polarization Ellipse and (B) the Poincaré Sphere of the LCP state.

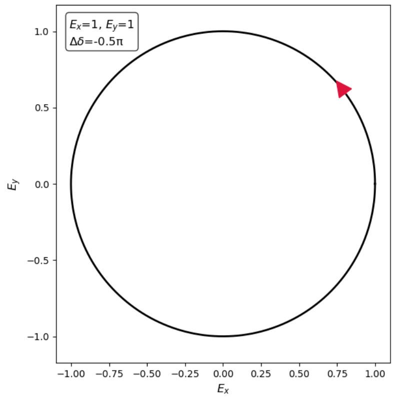

(A) Polarization Ellipse

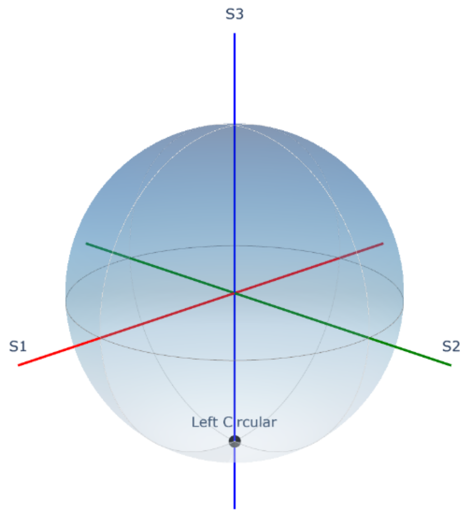

(B) Poincare Sphere

FIGURE 2.10: Circular left polarization state.(A) Polarization Ellipse. (B) Poincaré Sphere.

2.2. Historical overview of polarimetric optical fiber sensors

The investigations of polarized light began with the discovery by Erasmus Bartholinus in 1669 of the phenomenon of double refraction in calcite crystals (calspar).

Christian Huygens first proposed that light is not a scalar quantity in his Traité de la Lumière, based on his studies of light propagation in crystals. This vectorial nature – which Isaac Newton described as light having ”sides” – is what we now call polarization and arises because a light wave consists of only two transverse components.

The polarization of light was first explained by Augustin Jean Fresnel (1788–1827) and his successors when they introduced the wave theory of light, which also explained the major optical phenomena of interference and diffraction. This theory was only able to describe completely polarized light [5].

It was only in 1852 that Sir George Gabriel Stokes provided the mathematical formulation for describing any state of polarized light and for unpolarized light [6].

Due to the work of all these scientists, the polarization of light is a well-known phenomena and a crucial aspect of light in many applications. With the appearance of optical fibers, this characteristic of light became even more interesting, because of the properties of the fibers that make it possible to use polarization as a sensing tool, shown by Kaminow [7].

Since the work of Kaminow in 1981, many investigators have continued his work and perfected it. Ryo in 1991, published a paper about the application of optical fibers submarine cables, developing the first sea trial of a coherent frequency-shift-keying (FSK) system [8]. And a decade later, Waddy measured the state of polarization (SOP) in an aerial fiber during winter and summer. He made correlations the SOP changing and the current weather to search for the reason of the fastest SOP fluctuations, this allowed to better understand how perturbations in the fiber affect the polarization [9].

These early works created a base of knowledge, however the use of SOP for sensing did not have much interest because it was very difficult to implement and the alternatives seemed more appealing.

In 2013, Palmieri published a paper where he reviewed the field, putting emphasis on its underlying principles and unique applications, such as magnetic field mapping and twist measurement [10]. The SOP was measured for back-scattered light in respect to temperature, lateral stress, bending, twist and magnetic field. This paper laid the ground for future works by giving an overview of the most important concepts in SOP sensors. In his work he proposed two possible approaches to polarization-based Distributed Optical Fiber Sensors (DOFSs), as shown in Fig. 2.11. A polarizer is interposed between the reflectometer and the fiber to convert SOP variations of the backscattered light in power fluctuation (Fig. 2.11 a); polarization controller and a polarization analyzer are inserted in the input and output paths, allowing for a complete polarimetric characterization of roundtrip propagation (Fig. 2.11 b).

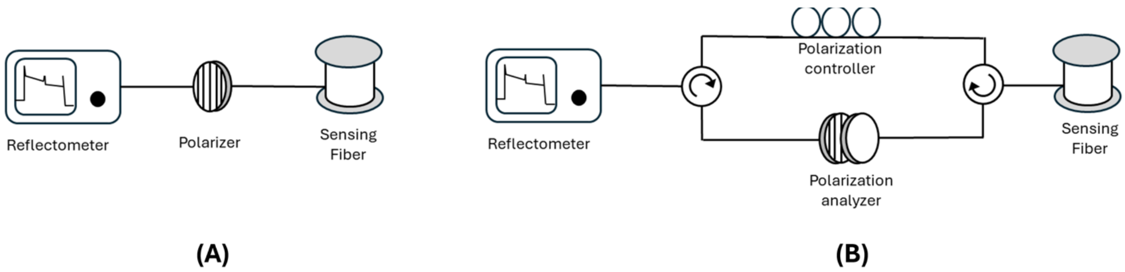

FIGURE 2.11: Setups used for polarization-based DFOSs.
(A) A polarizer placed between the reflectometer and the fiber converts SOP variations of the backscattered light into power fluctuations.
(B)A polarization controller at the input and a polarization analyzer at the output enable complete polarimetric characterization of round-trip propagation.

In recent years, several papers have been published and active research started in this area of knowledge. Most of this papers focus on the use of a polarization based sensor using submarine cables, since in the bottom of the ocean there are not as many perturbation as in aerial cables, resulting in a more stable signal. They also define the perturbation using the birefringence of the optical fiber, highlighting how important this property of the fiber is when used as a polarimetric sensor.

In early 2021, Zhan presented sensing results of seismic and water waves over a 10,000 kilometer-long submarine cable connecting Los Angeles, California, and Valparaiso, Chile, by monitoring the polarization of regular optical telecommunication channels [11]. In this paper, Zhan highlighted how the study of submarine earthquakes using seafloor geophysical instrumentation is challenging to deploy and maintain, and how fiber-optic sensing technologies that can leverage submarine telecommunication cables present an opportunity to fill the information gap. In the same year, Mecozzi et al. published a paper with similar objectives, where SOP was used to detect seismic activity, using the birefringence of the fiber, creating spectrograms that exhibited the changes when a perturbation occurred [12]. Later, in 2024, Mecozzi et al. presented work also focusing on SOP sensing using submarine cables, but with a more in depth analysis of the theoretical framework and the distinct advantage of polarization over phase in detecting sub-hertz environmental processes [13]. A scheme capable of extracting the spectrum of perturbations affecting a specific section at any position along an optical fiber by detecting the state of polarization of the backreflected light was proposed. It is important to note that both Zhan and Mecozzi compared SOP sensing with DAS (Distributed Acoustic Sensing), emphasizing how SOP is more effective in distributed sensing.

In 2023, Costa et al. showed that the current techniques capable of interrogating the entire length of transoceanic fibers are either incompatible with conventional telecommunication lasers or are limited in their ability to identify the position of the seismic wave. Also, he demonstrated a method to measure and localize seismic waves in transoceanic cables using only conventional polarization optics, by launching pulses of changing polarization [14]. He measured and localized seismic waves from a earthquake in Guerrero, Mexico using a submarine cable connecting Los Angeles, California and Valparaiso, Chile.

Mazur et al. was the first to use a real-time coherent transceiver with built-in real-time phase and polarization sensing while simultaneously transmitting information [15]. To describe the perturbation, he used correlation function of Jones matrices. This new approach enabled sensing in real time is possible using phase and equalizer outputs over 12800km of a submarine cable, enabling time resolved spectroscopy in a broad spectral range. The real time sensing capabilities of the setup prototype allowed the detection of swells and the monitorization of a 524km live network link during a human-caused cable break [16]. Post-analysis of polarization data uncovered potential warning signals at a minute-level scale, revealing deviations from baseline levels that occur immediately before the break.

All these works pretend to demonstrate that polarization sensing using submarine cables is a viable and innovative way to measure perturbations in the deep ocean. Compared to DAS and other standard methods, SOP has several advantages but also many limitations that must be overtaken in order to be a reliable technique for seismic detection.

3. Study of polarization effects in Erbium-Doped Fiber Amplifiers

In the 1980s, H. J. Shaw and Michel Digonnet invented the first fiber-optic laser amplifier at Stanford University in California [17]. The erbium-doped fiber laser amplifier (EDFAs) was created a few years later [18], and has become one of the most important fiber amplifiers when it comes to long-distance fiber optic communications. Due to their ability to efficiently amplify light in the 1550 nm region (the preferred wavelength for optical fiber communication, because it coincides with the third transmission window of silica optical fibers), EDFAs are widely used today in the field of optical communications over long distances or with high data transmission rates.

Studying polarization in EDFA systems is crucial for both research and industrial applications involving optical communication [19][20]. Several factors contribute to this importance, one of the most significant being Polarization-Dependent Gain (PDG) [21]. EDFAs are not perfectly isotropic; in erbium-doped fibers, the gain can depend on the state of polarization (SOP) of the input light [22]. This means that different polarization states may experience different levels of amplification, resulting in gain fluctuations that limit the stability of the output power.

Polarization Dependent Gain (PDG) is the unwanted phenomenon where the gain (amplification) of an optical component varies depending on the SOP of the incoming light signal and can be calculated using the input and output power, by means of Eq. 3.1, where $G = P_{out}/P_{in}$. .

$$PDG = G_{max} - G_{min} \tag{3.1}$$

An ideal optical amplifier would provide the same level of amplification regardless of whether the input light is vertically, horizontally, or circularly polarized. However, due to microscopic asymmetries and imperfections in the materials, real-world components exhibit a slight preference for one polarization over another. Typical values for an EDFA range from $0.1dB$ to $0.5dB$.

Another important factor is Polarization-Related Noise [23], particularly Polarization Mode Dispersion (PMD) [24] [25]. PMD causes the two orthogonal polarization modes of light to travel at different speeds, which induces pulse broadening. This makes the pulse wider and with a lower power peak, which is problematic for the transmission of information.

Although EDFAs are not the primary source of PMD, they can amplify its effects along the fiber, especially in long-haul systems. PMD can lead to signal distortion and degradation of system performance over distance. Therefore, polarization studies help mitigate the cumulative effects of dispersion and improve system reliability.

This chapter investigates the phase variation of light as a function of optical amplification. The Stokes vectors at the fiber output were measured using a polarimeter, an instrument that determines and records the state of polarization.

3.1. Characterization of EDFA

In EDFAs, as in conventional lasers, optical amplification occurs by stimulated emission. When the amplifier is pumped by a laser to achieve population inversion, the gain is attributed to the excited Er^{+3} ions. In the stimulated emission process, the energy from the pumping laser is transferred to the signal when the dopant ions are excited by the absorption of photons supplied by the pumping laser. Subsequently, these ions transmit this excess energy to the signal. However, noise photons, emitted randomly by spontaneous decay of initially negligible atoms that have been excited, are also amplified. This phenomenon is referred to as amplified spontaneous emission (ASE), and it constitutes an integral component of the noise inherent in all amplifier systems.

To account for amplifier saturation—a prevalent phenomenon resulting from excited-state depopulation by high signal photon numbers—the gain coefficient (g) is expressed as a function of the small-signal gain $g_0(\lambda)$, the signal power P, and the saturation power P_s (Eq. 3.2):

$$g = \frac{g_0}{1 + P/P_s} \tag{3.2}$$

To study the phase variation of light as a function of optical amplification, a commercial erbium-doped fiber laser amplifier was coupled to an adjustable signal laser and an power-meter, as shown in figure 3.1.

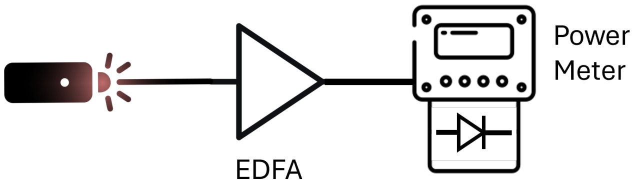

FIGURE 3.1: Experimental setup used to characterize the amplifier.

In order to obtain the laser amplifier's characterization curves and to observe the saturation phenomenon, the amplification of the output signal as a function of the pumping power was studied for two input signal levels, and the gain as a function of the input signal power, was also studied for two pumping power levels.

The dependence of gain on amplifier power for two input signal levels is shown in Fig. 3.2. An initial saturation behavior is observed as the input power increases. However, the saturation regime was not reached under these conditions.

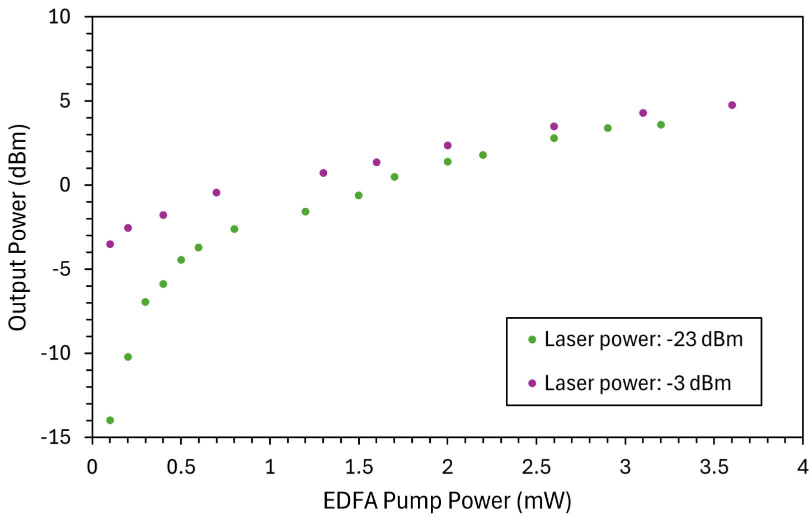

FIGURE 3.2: Signal gain as a function of the output power of the EDFA for two different laser input powers: -23 dBm; -3dBm..

The power of the input signal was varied, for a fixed pumping power, as shown in Fig. 3.3. From this, it is possible to determine how the range of the signal should be restricted in order to obtain greater amplification. It was concluded that the amplification is greater for lower laser powers.

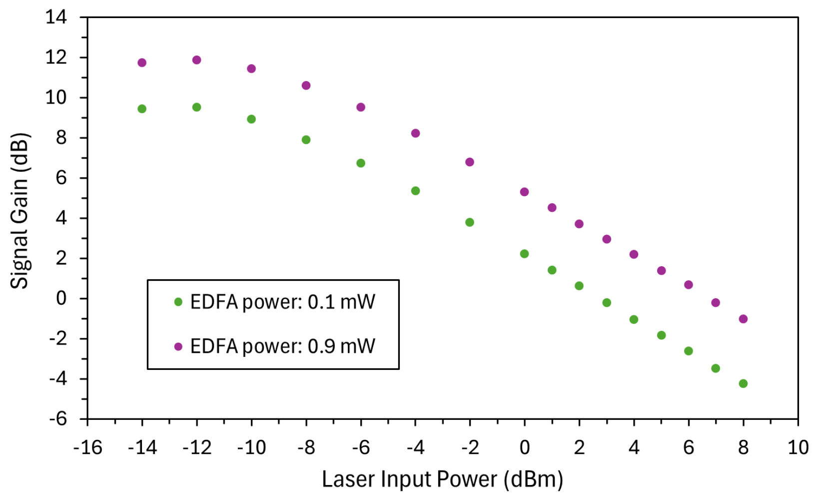

FIGURE 3.3: Signal gain as a function of the laser output power for two different EDFA input powers: 0.1 mW and 0.9 mW.

3.2. EDFA configuration for short distances

The experimental configuration is illustrated in Fig. 3.4. In this setup, the optical power was modulated using a tunable semiconductor laser (Santec), operating at a wavelength of 1550 nm, in conjunction with an EDFA (Multiwave). A polarimeter (Novoptel) was employed to monitor the State of Polarization (SOP) and to analyze the corresponding phase variations. Nevertheless, several challenges arose due to the inherently unpredictable behavior of polarization, particularly in short fiber segments where external perturbations and birefringence are more pronounced.

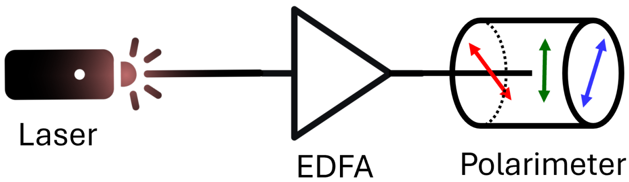

FIGURE 3.4: Setup used to study the polarization effects for a standard EDFA configuration.

One notable limitation was the occurrence of saturation in the polarimeter. As a result, the laser power could not be set too high, especially considering the limited dissipation capacity in short fiber lengths. Also, the laser power could not be very low, in order to have a stable signal. To explore the optimal conditions for stable measurements, three distinct laser power levels were tested using the Poincaré Sphere in the polarimeter:

- -18 dBm, representing the maximum laser power before saturation occurs in the polarimeter;
- -20 dBm, a power in the middle of the range of stable operation of the laser;
- -23 dBm, the minimum power that still ensured a stable and detectable signal.

The Stokes parameters were recorded across the full operational range of the EDFA for the three laser powers, starting with -18 dBm (Fig. 3.5). To assess hysteresis effects and verify the reproducibility of the results, the measurements were performed by ramping the EDFA input power up and down three times. Finally, the phase variation was calculated using Eq. 2.11.

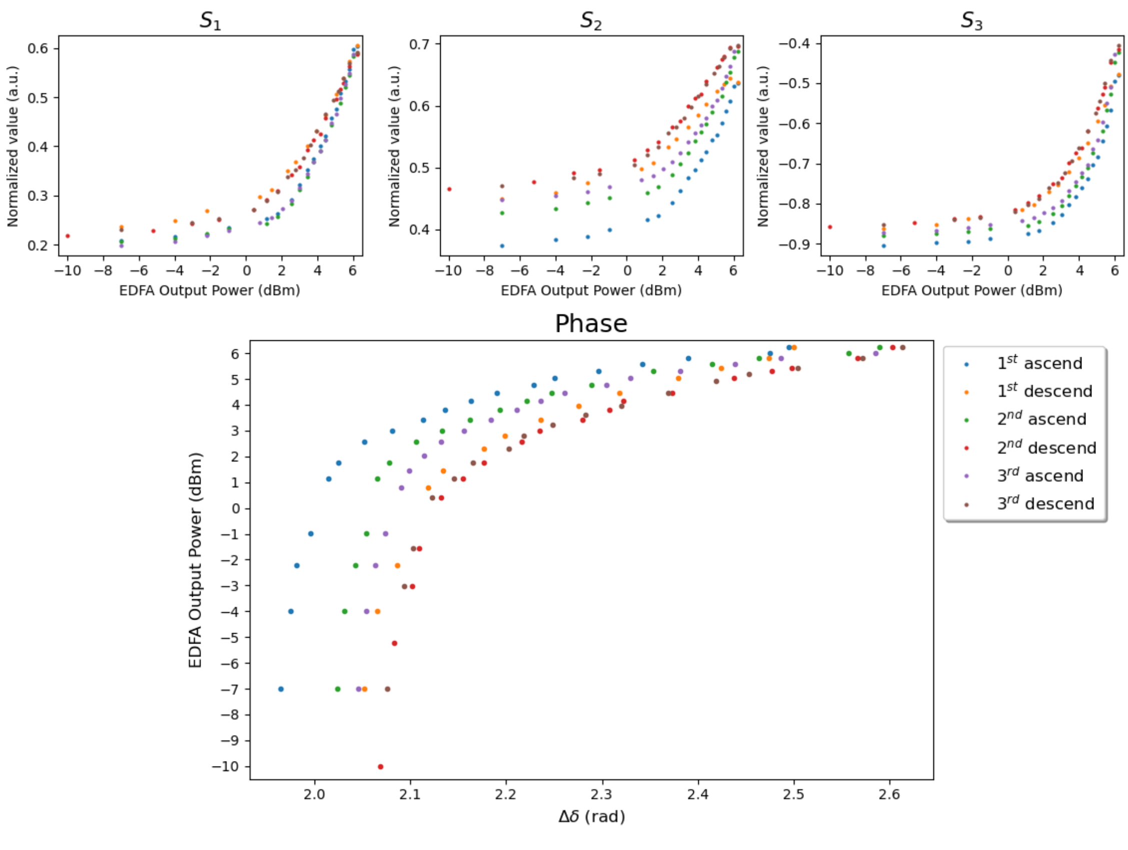

FIGURE 3.5: Stokes parameters (top) and light phase (bottom) as a function of the EDFA output power, for a laser power of -18 dBm.

In the phase results shown in Fig. 3.5, a slight phase shift can be observed across consecutive sweeps over the full operating range. However, the overall behavior remains consistent and demonstrates satisfactory repeatability.

The slight phase shift can also be observed in the Poincaré sphere, shown in Fig. 3.6.

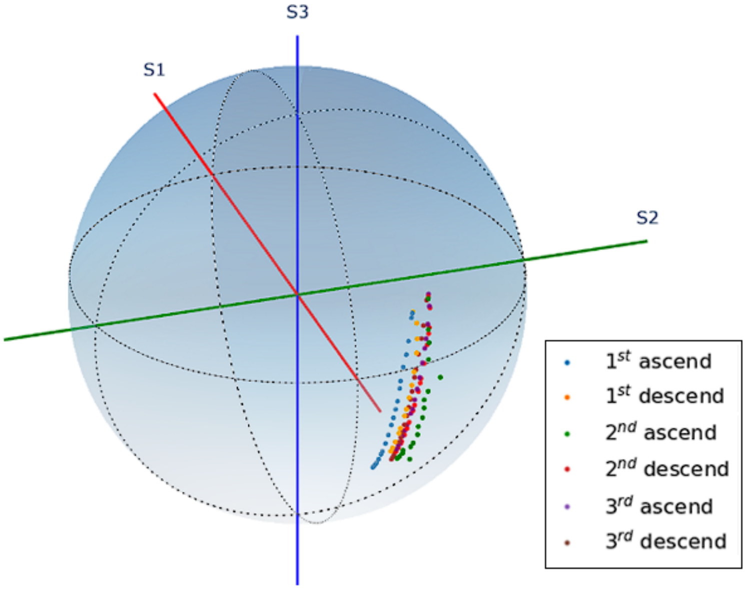

FIGURE 3.6: Poincaré sphere for a laser power of -18 dBm.

Since the range of stable operation of the laser was determined to be from -23 dBm to -18 dBm, data was recorded for approximately the middle of this range: -20 dBm.

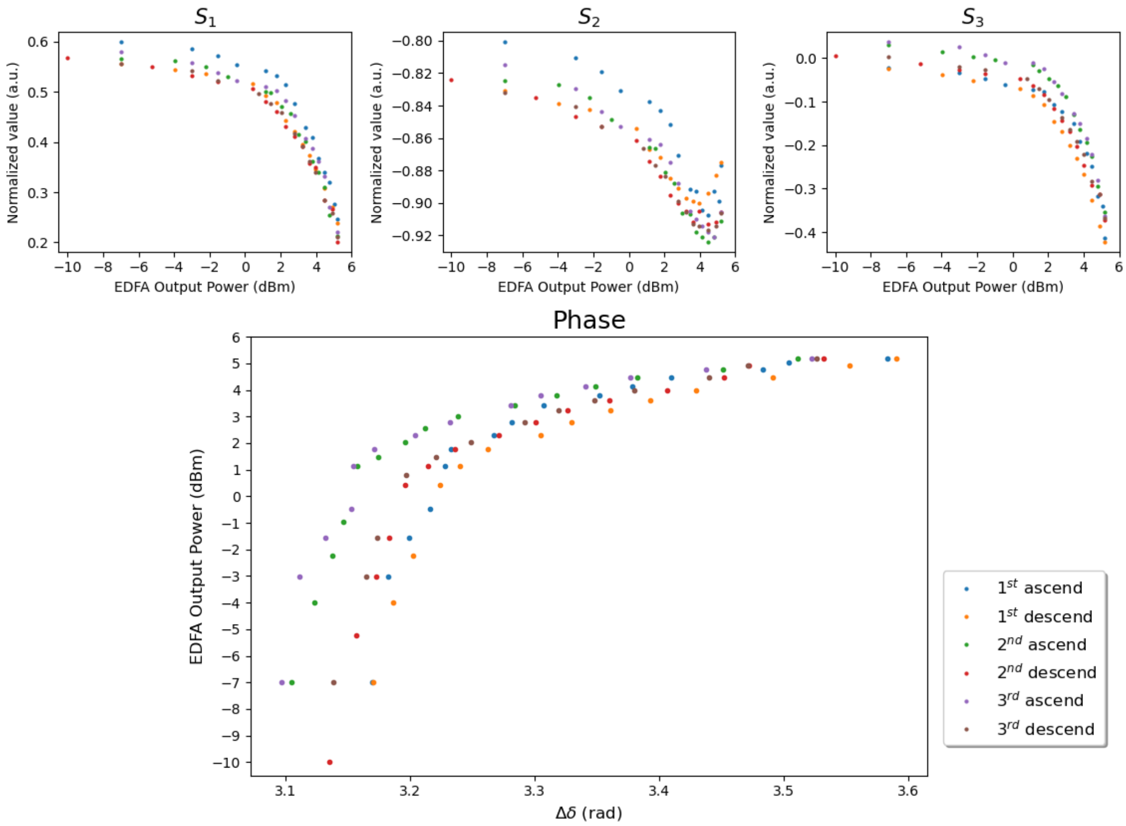

FIGURE 3.7: Stokes parameters (top) and light phase (bottom) as a function of the EDFA output power, for a laser power of -20 dBm.

Fig. 3.7 also shows satisfactory results, with similar behavior as observed from the Stokes parameters and calculated phase, considering laser power -18 dBm.

Once more, the slight phase shift can also be observed in the Poincaré sphere, shown in Fig. 3.8.

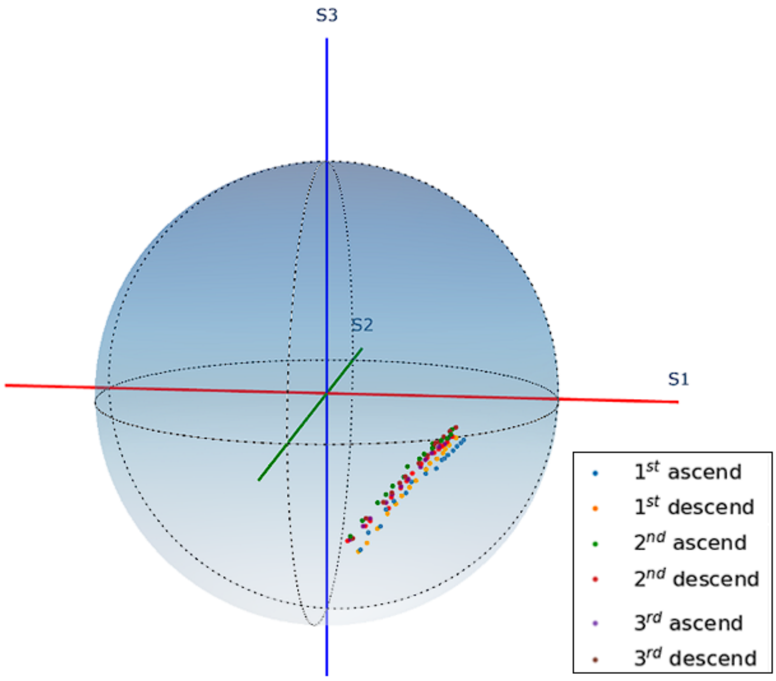

FIGURE 3.8: Poincaré sphere for a laser power of -20 dBm.

As previously mentioned, these measurements were also performed for the lowest laser power with signal stability. To obtain the lowest possible laser power that still ensured signal stability the power of the laser was gradually decreased and the polarization state on the Poincaré sphere — provided by the polarimeter software — was monitored. The minimum power ensuring stable operation was determined to be -23dBm. The corresponding results are presented in Fig. 3.9.

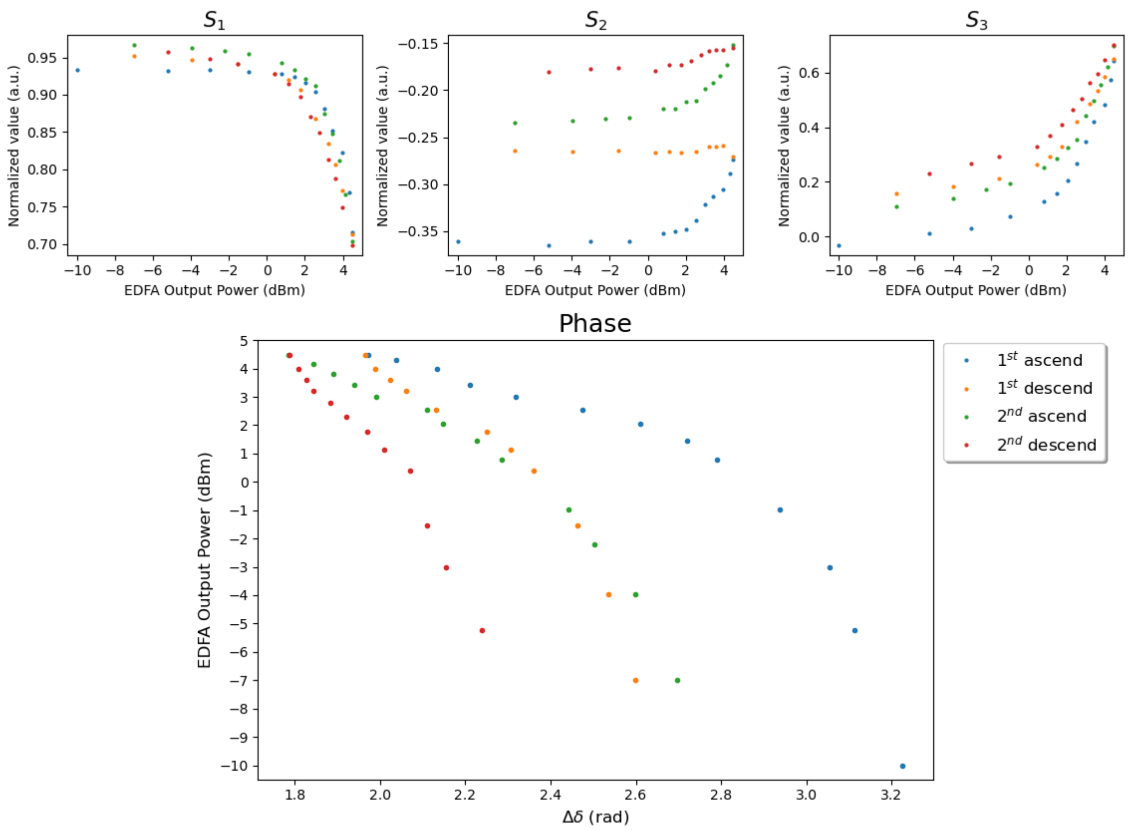

FIGURE 3.9: Stokes parameters (top) and light phase (bottom) as a function of the EDFA output power, for a laser power of -23 dBm.

Measurements of the full operational range were limited to two sweeps because the second sweep unequivocally demonstrated prominent phase shifting. The displacement is clearly observable in the phase measurement and is especially pronounced in the Stokes parameter S_2, where no overlap exists between points of identical power.

The Poincaré sphere is presented in Fig. 3.10, for better visualization of the data behavior.

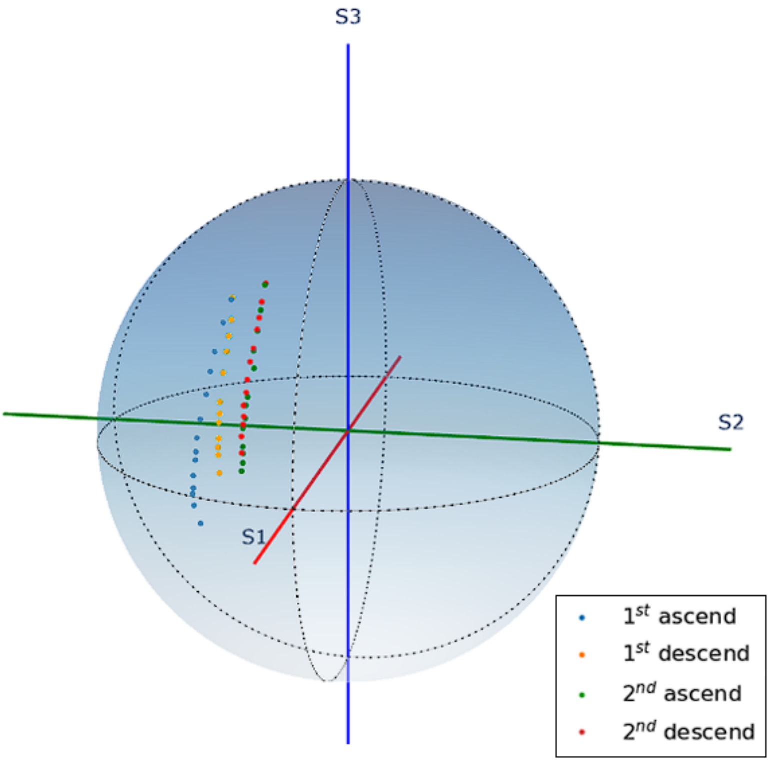

FIGURE 3.10: Poincaré sphere for a laser power of -23 dBm.

Finally, the polarization dependent gain was determined for laser powers tested is presented in Figs. 3.5, 3.7 and 3.9, using Eq. 3.1:

TABLE 3.1: Polarization-dependent gain calculated for all tested laser powers.

	-18 dBm	-20 dBm	-23 dBm
PDG	0.461 dB	0.463 dB	0.429 dB

The values determined for the polarization gain are very similar to each other, and are within the expected range for a commercial EDFA.

3.3. EDFA configuration for long distances

First, to understand how laser power affects the phase of light, a study was conducted on the polarization state as a function of laser power. This analysis helps identify the regions where the signal exhibits greater sensitivity and stability. The experimental setup used is shown in Fig. 3.11, with the EDFA turned **off**. The state of polarization (SOP) of the light was recorded across the entire operating range of the laser source. The phase was then calculated using Eq. 2.11.

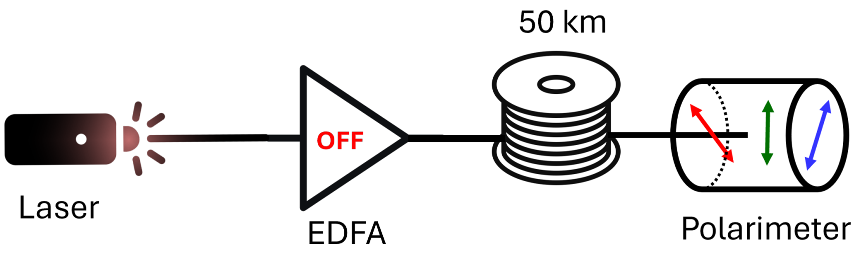

FIGURE 3.11: Setup used to study the polarization effects of the laser in a configuration for long distances.

This study revealed two distinct behavioral regions in the system response, as shown in Fig. 3.12. The first region (left), ranging from -20 dBm to -10 dBm, exhibits relative stability. This stability is attributed to the low input laser power and the absorption characteristics of the erbium-doped fiber, which dominates signal behavior in this range. In contrast, the second region (right), spanning from -10 dBm to 10 dBm, demonstrates a linear response.

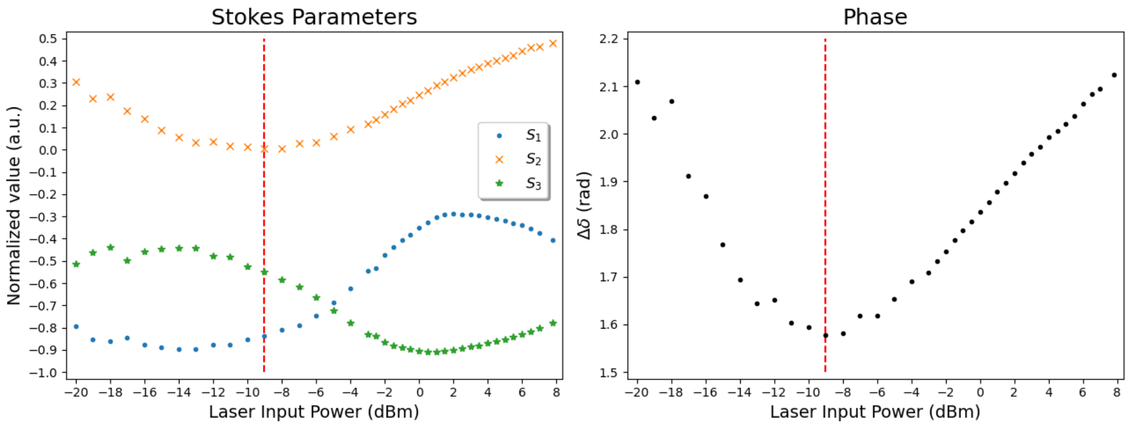

FIGURE 3.12: Stokes parameters as a function of the laser output power (left). Phase as a function of the laser output power (right).

These results demonstrate that higher input powers lead to stable signal transmission with consistent properties in the erbium-doped fiber, indicating no noticeable degradation. This stable operation suggests enhanced efficiency at elevated powers, where fiber absorption effects are minimized.

After the study on how the laser power affects the phase of the light, the EDFA was switched on and a study was conducted to averiguate its influence on the SOP. The configuration used is the same as with the amplifier switched on, as shown in Fig. 3.13.

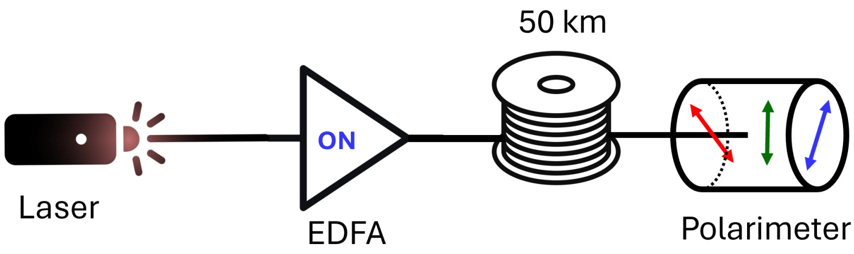

FIGURE 3.13: Setup used to study the polarization effects of the EDFA in a configuration for long distances.

To assess the consistency of the system's response, the output power fo the system was cyclically increased and decreased.

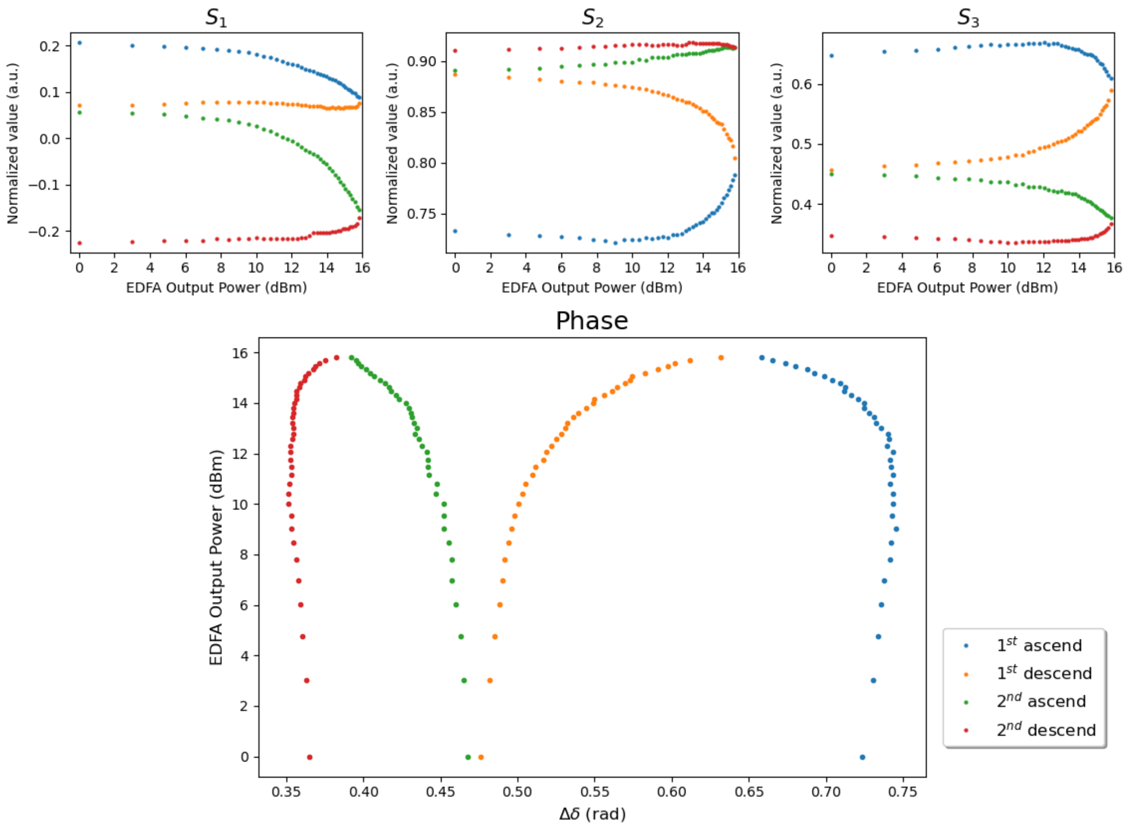

FIGURE 3.14: Stokes parameters (top) and light phase (bottom) as a function of the EDFA output power, for a laser power of 0 dBm.

The Fig. 3.14 clearly shows that the results are not consistent: for the same range of values, the results are significantly different. Moreover, it is very noticeable that the phase does not return to the initial state during the successive measurements. This is most likely due to a phase accumulation effect caused by the 50 km of optical fiber the light has to travel through. The 50 km of fiber, that are curled up, can have changes in temperature that are not uniform causing a not consistent phase accumulation.

This phase accumulation is also very apparent in the Poincaré sphere, shown in Fig. 3.15. In the sphere, there is clearly a continuous behavior, instead of the slight shift that was present in the previous data.

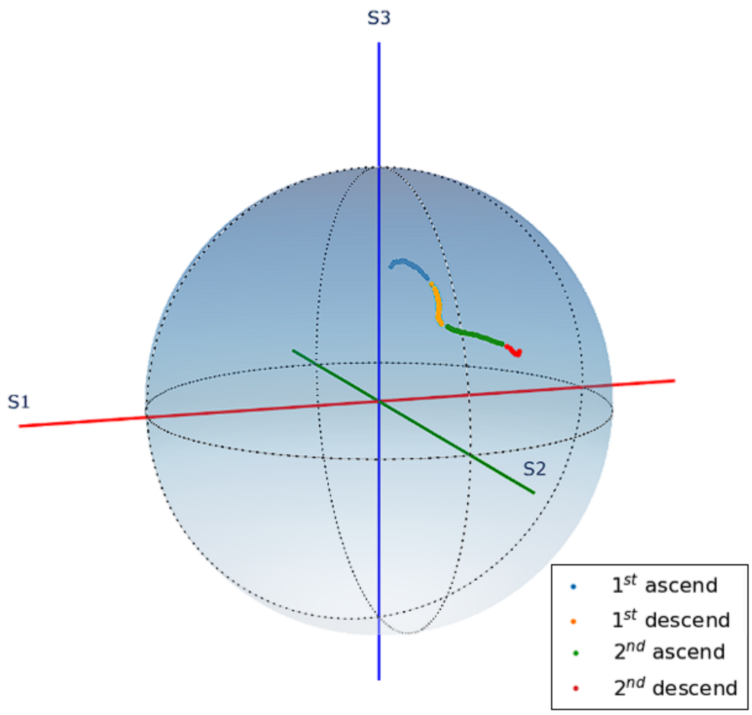

FIGURE 3.15: Poincaré sphere for a laser power of 0 dBm.

The polarization dependent gain was determined to be 0.477 dB, using Eq. 3.1, which is a similar value to the ones obtained in the previous section (Tab. 3.1).

3.4. Conclusions

In this chapter, a comprehensive study was conducted on the phase behavior of light and its response to amplification using a laser source in conjunction with an Erbium-Doped Fiber Amplifier (EDFA), under various operating conditions.

Initially, the influence of amplification on the optical phase was examined in a simplified setup. Three specific conditions were tested: (1) minimum power with a stable signal, (2) middle of the range of stable operation of the laser, and (3) maximum power without saturation. The results indicate that the optimal performance was achieved at a higher input power level of -18 dBm, which provided the most consistent phase response.

Following this preliminary analysis, a more realistic configuration was investigated, incorporating 50 km of optical fiber. It was found that the ideal operating range for the laser lies between 0 dBm and 2 dBm. However, these power levels are only suitable for long fiber spans; for shorter lengths, signal saturation becomes a limiting factor. Furthermore, a substantial phase drift was observed over the 50 km fiber span, rendering such lengths impractical without implementing phase compensation mechanisms.

In conclusion, the study demonstrates that optical power plays a critical role in determining both SOP and phase stability in optical fiber systems. Specifically, increased output power —particularly when EDFA amplification is employed— leads to more pronounced phase variations. These findings underscore the importance of precise power management in systems sensitive to polarization and phase changes.

4. Measure of physical parameters using a polarimeter

This chapter transitions from characterizing amplifier polarization to applying those principles for sensing physical parameters. Accurate measurement of parameters such as temperature and strain is critical for system characterization. Sensors function by detecting changes in a physical system and producing a corresponding output signal. The specific class of fiber optic sensors utilizes light transmission or reflection within the fiber to detect perturbations along its length. The work in this chapter focuses on a sensor operating in transmission.

Optical fiber sensors have attracted considerable attention due to the advantages such as compactness, light weight, high stability, repeatability, and immunity to electromagnetic interference. Polarimetric fiber optics sensors are classified as phase sensors, which are devices that detect phase shifts between two electric field components of a light. The transmission of light through a birefringent optical fiber results in a change in the polarization state of the output.

It has been demonstrated that light is susceptible to changes in output polarization when subjected to various forms of stress, including axial strain, twist, and other perturbations, which is the underlying reason for the significant potential of polarimetric fiber optic sensors [26].

In this chapter, a polarimetric sensor is presented based on a polarimeter, capable of detecting various perturbations in a optical fiber. The polarimeter allows detecting the Stokes parameters, that fully characterize the polarization. Only the S_2 and S_3 parameters are presented, since they are the ones that are relevant for the phase (Eq. 2.11).

4.1. Temperature sensor

Fiber optic temperature sensors are immune to electromagnetic environment effects that compromise other measurement technologies. In addiction to that, they can be embedded and installed in locations traditional sensors cannot. Unlike traditional thermocouples or resistance temperature detectors (RTDs), these sensors rely on light propagation and optical properties, making them resistant to electromagnetic interference (EMI), chemically inert, and capable of operating in extreme conditions [27].

Polarimetric temperature sensors are a type of fiber optic sensor that measures temperature-induced changes in the polarization state of light propagating through an optical fiber. These sensors exploit the birefringent properties of certain optical materials, which vary with temperature, allowing for thermal measurement [28].

In order to detect temperature changes using the polarimetric sensor, the room temperature was set to 19ºC using an air conditioner (AC). To start the measurements, the air conditioning system was deactivated to allow for a gradual rise in ambient temperature within the room. The local temperature of the fiber was recorded using a digital thermometer. It was evident that this configuration is sub-optimal due to the presence of other equipment and individuals within the laboratory which introduce variability in temperature fluctuations. The setup used is shown in Fig. 4.1. The EDFA studied in Chapter 3 was used in this experiment, so that the input signal arrived to the polarimeter with enough power after 50 km of propagation, as well as the polarimeter to measure the SOP.

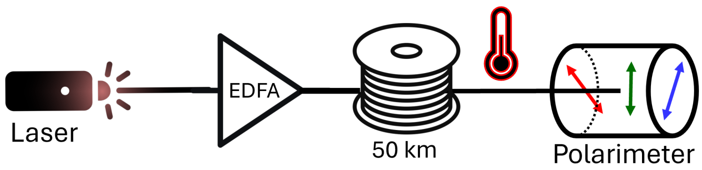

FIGURE 4.1: Experimental setup used to measure temperature changes.

By monitoring the temperature with the digital thermometer, the Stokes parameters were recorded from 19.7ºC to 22.4ºC, and the phase was then calculated using Eq. 2.11.

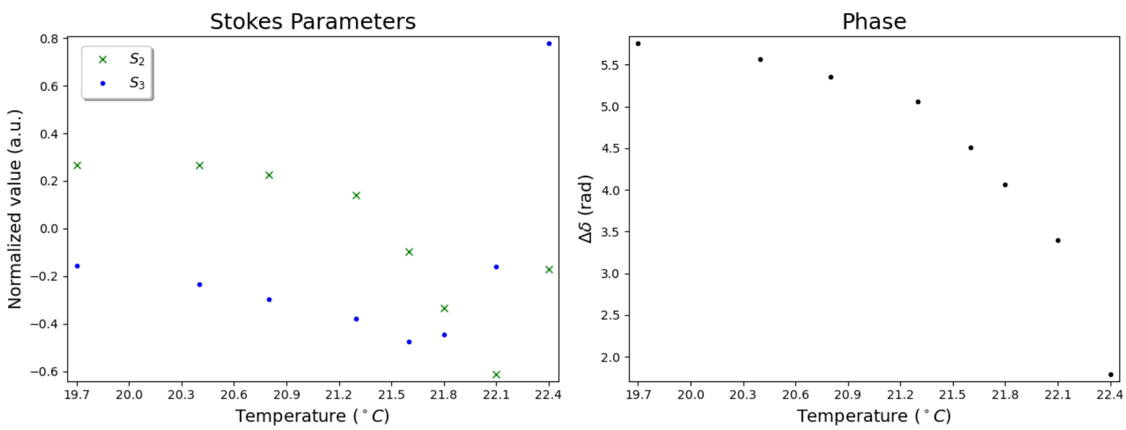

FIGURE 4.2: Stokes parameters (left) and light phase (right) as a function of room temperature.

S_1 was not shown because Eq. 2.11, used to calculate the light phase, depends only on S_2 and S_3. Although the temperature change is small, the sensor can clearly detect this variation.

4.2. Polarimetric twist sensor

Optical fiber twist sensors are advanced devices that measure torsional deformation, rotation, or twist using the principles of light propagation in optical fibers [29]. These sensors leverage changes in light properties—such as intensity, phase, polarization, or wavelength—to detect and quantify twisting forces. Due to their high sensitivity, immunity to electromagnetic interference (EMI), and compact size, they are widely used in structural health monitoring, robotics, aerospace, and biomedical applications. Common detection mechanisms include: Fiber Bragg Gratings (FBG) [30], Helical Long-Period Fiber Gratings (HLPGs) [31], interferometric sensors [32], and polarimetric sensors [33].

On the other hand, polarimetric twist sensors are a specialized class of optical fiber sensors that measure torsional deformation by analyzing changes in the polarization state of light propagating through an optical fiber [34]. These sensors operate based on twist-induced birefringence in optical fibers. When the fiber is twisted, mechanical stress modifies its refractive index asymmetrically, altering the polarization state of transmitted light.

The experimental configuration used in this study is illustrated in Fig. 4.3. The initial polarization state, corresponding to no applied twist, was set to linear via a polarization controller. The optical signal was amplified by the EDFA previously studied in Chapter 3. A 0.45 meter segment of the fiber was subjected to torsion using a custom twisting apparatus, and the corresponding Stokes parameters were recorded throughout the process using a polarimeter.

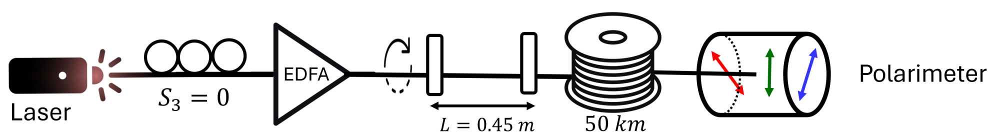

FIGURE 4.3: Setup of the polarimetric twist sensor.

The fiber section under study was twisted through 360°— one full turn — in 15° steps, as shown in Fig. 4.4. The Stokes parameters recorded by the polarimeter were converted to phase using Eq. 2.11 once again.Once more, only S_2 and S_3 are presented.

The Stokes parameters change periodically with the applied twist. The phase changes with the variation of the twist angle and shows sinusoidal behavior.

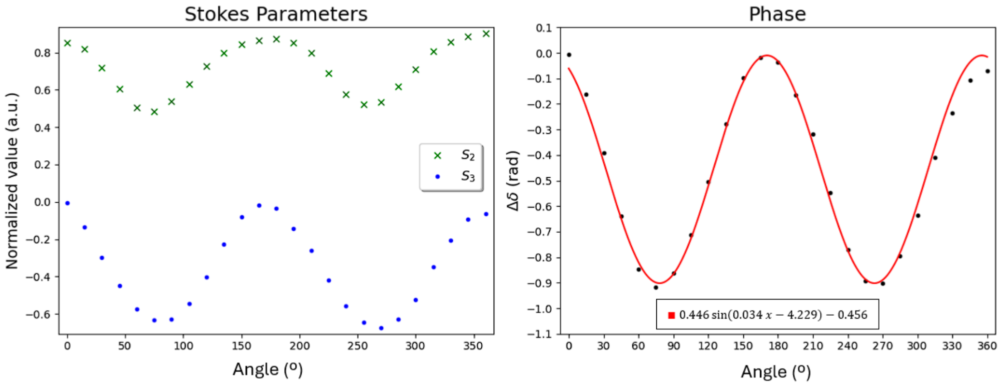

FIGURE 4.4: Stokes parameters (left) and phase (right) as a function of the twist applied to a 0.45 m section of optical fiber.

In the context of a torsion sensor, the phase should be the same for each half turn (180º). However, the contraption used to induce the twisting motion can introduce an error. Since the phase after 180º and 360º is a little deviated from the initial phase (0.03 rad and 0.06 rad, respectively), it can be concluded that the sensor has a calibration shift of approximately 0.03 rad.

Despite the small phase shift present in the results, these findings demonstrate that the experimental setup possesses strong potential for accurately sensing the twist of optical fibers.

4.3. Polarimetric strain sensor

Strain is defined as a measurement of deformation, representing the relative displacement between particles in a material under applied stress. This measurement quantifies the degree to which an object's shape is altered, with higher values indicating greater stretching, compression, or distortion from the object's original form.

This physical quantity is dimensionless and is usually calculated using Eq. 4.1, where L is the original length of the fiber being stretched and ΔL is the change in length induced in the fiber.

$$\varepsilon = \frac{\Delta L}{L} \tag{4.1}$$

Although strain is unitless, it is often reported in microstrain: $\mu\varepsilon = \varepsilon \times 10^{-6}$. In this chapter this is how strain will be expressed.

Optical fiber strain sensors are devices that measure mechanical strain in structures by analyzing changes in light propagation through an optical fiber [35]. There are many types of strain fiber sensors: Fiber Bragg Grating (FBG) Sensors [36]; Long-Period Fiber Grating (LPFG) Sensors [37]; Interferometric Sensors [38][39]; Distributed Fiber Optic Sensors [40]. Although these sensors have a lot of advantages such as long distance monitoring, and high sensitivity and durability, there are also some challenges associated with them, namely the complexity of their installation and the cost of interrogators, especially for high-resolution distributed sensing.

On the other hand, polarimetric strain sensors are a type of optical fiber sensors that measure strain by detecting changes in the polarization state of light propagating through the fiber. These sensors rely on birefringence — difference in refractive indices for two orthogonal polarization modes — induced by mechanical stress. These sensors, while still having high sensitivity and immunity to EMI, do not require additional installation costs if an optical fiber is already installed. However, they need a complex signal demodulation and are susceptible to other external perturbations.

The polarimetric sensor employed in this study of strain is shown in Fig. 4.5. As was done in the previous section, the initial state was set to linear polarization ($S_3 = 0$) and the signal was amplified using the same EDFA. A 0.45 m section of the total 50 km of fiber was subjected to strain by gradually stretching it using a translation stage.

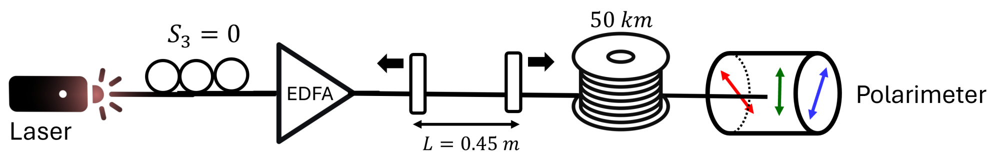

FIGURE 4.5: Setup of the polarimetric strain sensor.

The fiber segment under study was stretched in 20 μm increments until a total elongation of 1000 μm was reached. This corresponds to a strain ranging from $0\mu\varepsilon$ to approximately $2.2\mu\varepsilon$. The Stokes parameters were obtained using the Novoptel polarimeter, and the phase was plotted using Eq. 2.11. Figure 4.6 shows the relevant Stokes parameters (S_2 and S_3) used to determine the phase.

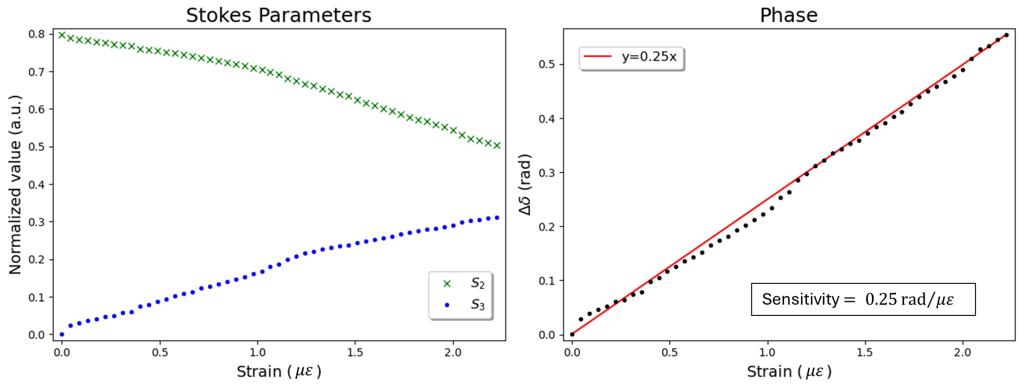

FIGURE 4.6: Stokes parameters (left) and phase (right) as a function of the strain applied to a 0.45 m section of optical fiber.

By analyzing the results shown in Fig. 4.6, it is very clear that the phase has a linear behavior in function of the strain with a slope of 0.25 rad $\mu\varepsilon^{-1}$. These results are satisfactory and demonstrate that this setup can accurately sense strain applied to optical fibers, making it a viable sensing solution.

4.4. Conclusions

In this chapter, a study of the sensing capabilities of a polarimetric sensor was conducted, for various physical parameters. The polarimetric sensor was employed using a polarimeter, a tunable laser, and 50 km of fiber.

Firstly, the stability of the sensor was tested, and it was concluded that after 30 minutes with the laser on the signal stabilizes, and measurements can be made.

After guarantying the stability of the sensor, three different studies were made to demonstrate the sensing capabilities of the polarimetric sensor: temperature, twist, and strain.

In the temperature study, even though the setup used was not ideal and could induce some errors, it was still possible to observe a trend. It was concluded that the sensor is capable of detecting temperature changes.

The sensing capabilities of the polarimetric sensor to the torsion of the fiber were demonstrated. It was expected that the light phased changed periodically for every half turn. However, it was concluded that the setup utilized had a calibration shift of approximately 0.03 rad, since there was a phase deviation for torsions of 180º and 360º in regards of the initial phase. Overall, the polarimetric sensor has capabilities to sense the twist of optical fibers.

Finally, when testing the strain sensing potential, it was proved that the phase has a linear behavior in function of strain. A sensitivity of $0.25\,\mathrm{rad}/\mu\varepsilon$ The results demonstrate the sensing capabilities of the polarimetric sensor to test strain.

All in all, the polarimetric sensor is able to sense the three physical parameters studied with satisfactory accuracy. In order to make it a viable multi sensor, some adjustments can be made to improve the accuracy.

5. Fiber Loop Mirror

In this chapter, a Fiber Loop Mirror (FLM) is used for two different applications: enhancing the sensitivity of the strain sensor developed in section 4.3; development of a rotation sensor to use as a proof of concept gyroscope. FLMs are used for a lot of applications, including: optical switching [41]; wavelength demultiplexing in optical communications [42]; sensing[43].

Although the sensing capabilities of the sensor developed are satisfactory, the sensitivity may be increased by using an high-birefringence (hi-bi) fiber, and by increasing the interaction length. One way to increase the interaction length is by reading in reflection.

A simple way to create a reflecting device in fiber optics is to form a fiber loop using a 2×2 directional fiber coupler, where the ports on one side are connected to each other with a short piece of fiber. A typical hi-bi fiber loop mirror is shown in Fig. 5.1 [44].

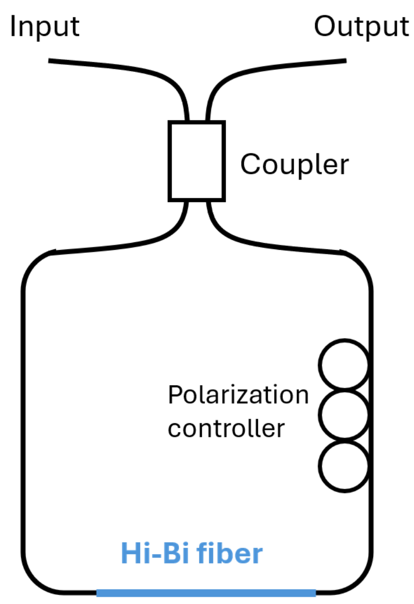

FIGURE 5.1: Scheme of an Hi-Bi fiber loop mirror.

By feeding light into one input port, the power is split so that two counterpropagating waves are formed in the loop. When these waves come together again at the coupler, they interfere with each other. This interference determines the optical power sent back into the input port as well as the power leaving the other port. The interference conditions can in general be influenced by various aspects such as multimode behavior, polarization changes and nonlinear effects.

Strictly speaking, such a fiber loop should be called a fiber loop reflector, but the more often used term is a fiber loop mirror. The fiber loop reflector can also be considered as a Sagnac interferometer, although the Sagnac effect is in many cases not utilized.

5.1. Enhancing the sensitivity of the strain sensor

In order to harness the advantages of the fiber loop mirror to use in a strain sensor, the portion of hi-bi fiber in the fiber loop mirror (Fig. 5.1) was submitted to strain, as shown in Fig. 5.2.

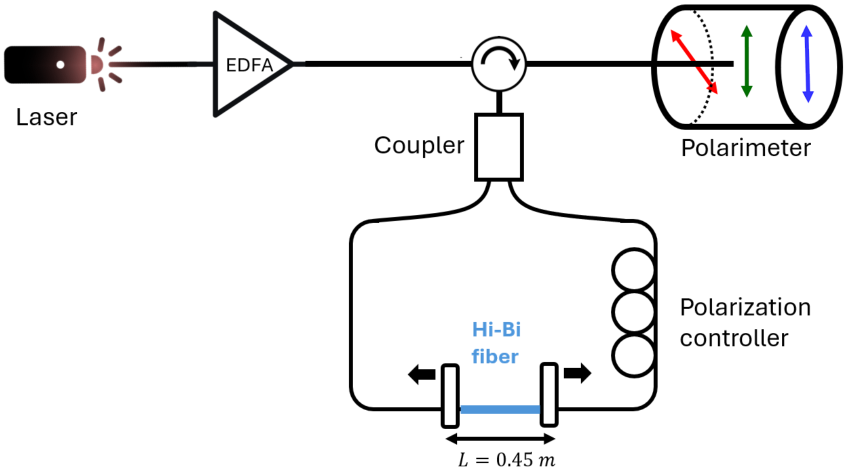

FIGURE 5.2: Setup of a polarimetric strain sensor integrating a fiber loop mirror.

Before starting measurements, the impact of the SOP of light in the spectrum of light was observed using an Optical Spectrum Analyzer (OSA). As expected in an optical cavity, the output spectrum consists of fringes and the laser peak. Changing the polarization causes the laser peak to move within the spectrum. When aligned with the top of a fringe, resonance occurs and a single larger peak appears. In this study, two different spectra were tested for the strain sensor: the first with the laser peak placed in the midle of the sploe of a fringe (Fig. 5.3a); and the second with the laser peak positioned at the top of the fringe (Fig. 5.3b). It is expected that better results will be obtained for the higher output intensity, that is, with the laser peak at the top of a fringe.

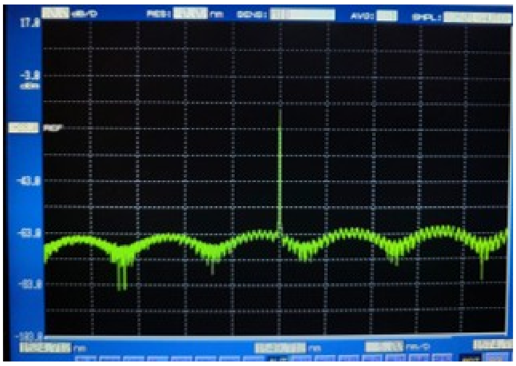

(A) Laser peak at the midle of the slope of a fringe.

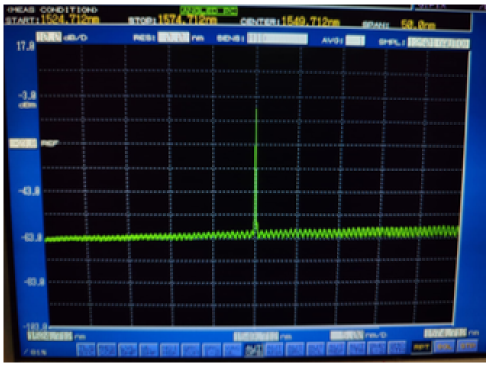

(B) Laser peak at the top of a fringe.

FIGURE 5.3: Output spectrum for two initial polarization states. (A) Laser peak at the midle of the slope of a fringe. (B) Laser peak at the top of a fringe.

After setting the state of polarization so that the spectrum appeared, as shown in Fig. 5.3a, strain was applied using the setup shown in Fig. 5.2. The 0.45 m of hi-bi fiber was stretched a total of $500\mu m$ with increments of $20\mu m$. This means that the maximum strain applied was half the one applied in the previous section 4.3. In Fig. 5.4, the behavior of the Stokes parameters (S_2 and S_3) and the phase of light (equation 2.11) are presented as a function of the strain applied.

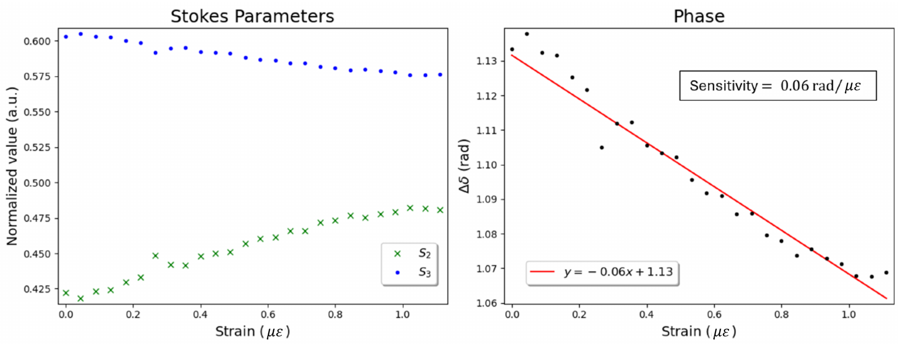

FIGURE 5.4: Stokes parameters (left) and phase (right) as a function of the strain applied to a 0.45 m section of optical fiber in an FLM. The laser peak is placed in the midle of the slope of a fringe (Fig. 5.3a).

As expected, the phase has a linear tendency, however the slope is negative and not very steep (-0.06 ± 0.01 rad $\mu\varepsilon^{-1}$), contrary to the curve presented in Fig. 4.5. This is something to have in consideration when using polarimetric sensors, since the initial SOP can influence greatly the behavior of the phase.

In order to compare and test the influence of the initial SOP in this setup, the exact same measurements were performed and plotted in Fig. 5.5, for the output spectrum shown in Fig. 5.3b.

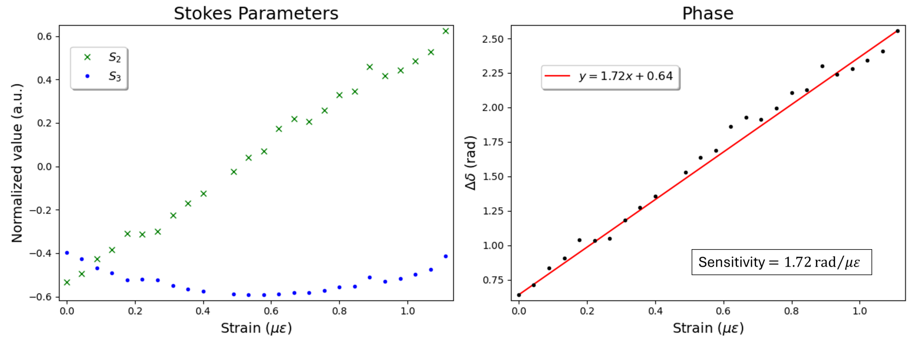

FIGURE 5.5: Stokes parameters (left) and phase (right) as a function of the strain applied to a 0.45 m section of optical fiber in an FLM. The laser peak is positioned at the top of a fringe (Fig. 5.3b).

Once again, the phase is linear as a function of strain, and has a positive slope (1.72 ± 0.01 rad $\mu\varepsilon^{-1}$). This behavior was also observed in the results presented in section 4.3.

In order to better visualize these two results, a plot of the SOP in the Poincare sphere was made, as is presented in Fig. 5.6. Comparing the two results it is very clear that the range of the sensor is very different depending on the initial polarization state. It is observed in Fig. 5.6a that the data in very concentrated in a small part of the sphere. However, in Fig. 5.6b, the data covers a large portion of the sphere. This is likely due to the very different sensitivities depending on the initial spectrum.

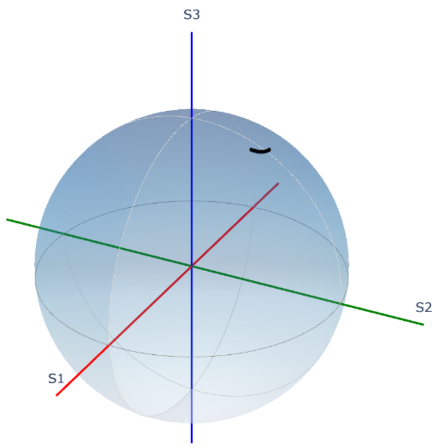

(A) Laser peak at the midle of the splope of a fringe.

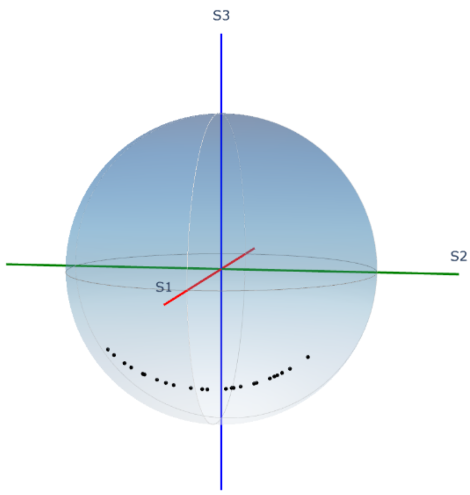

(B) Laser peak at the top of a fringe.

FIGURE 5.6: Poincaré sphere for strain applied to a 0.45 m section of optical fiber in an FLM. (A) Laser peak at the midle of the splope of a fringe; (B) Laser peak at the top of a fringe.

In fact, comparing the slopes of the phase curve as a function of strain for the three graphs —Fig. 4.6, Fig. 5.4 and Fig. 5.5 —, it is apparent that the sensitivity is greater for the setup with the fiber loop mirror and the peak on top of the fringes, since the slope is higher. In addition to that, it is also worth noticing that the sensitivity is better in the simple setup used for strain in Fig. 4.5 than for the fiber loop mirror with the peak in the middle of the fringe –Fig. 5.3a–, which proves that the fiber loop mirror can enhance the sensitivity of the sensor, but only for a controlled initial configuration.

In summary, the fiber loop mirror has been proven to enhance the polarimetric sensor developed, but only for certain initial polarization states.

5.2. Rotation sensor using a fiber loop mirror

Now that the fiber loop mirror was tested, and it was concluded that it enhances the sensitivity of the polarimetric sensor, this setup may be used –with some modifications– to develop a rotation sensor. This rotation sensor is essentially a gyroscope, but limited to one direction of rotation.

Gyroscopes are devices that measure or maintain orientation and angular velocity based on the principles of conservation of angular momentum. They are foundational technology for modern navigation, stabilization, and motion sensing. There are many types of gyroscopes, each with its advantages and disadvantages [45][46].

Mechanical Gyroscopes are the traditional type with a spinning mass on gimbals, they are very accurate but contain moving parts that can wear out. MEMS (Micro-Electro-Mechanical Systems) gyroscopes are tiny, chip-based gyroscopes found in phones, drones, and cars, that instead of using spinning wheel, use a vibrating mass that is affected by the Coriolis effect when the device rotates [47]. Although they are cheap, small and consume low power, they suffer from drift over time. Optical Gyroscopes have no moving parts, depending only on the properties of light [48]. There are several types of optical gyroscopes, and they normally are used in high-end navigation systems, due to their high accuracy and reliability.

A more relevant gyroscope is a Fiber-Optic Gyroscope (FOG), that measures rotational rate using the interference of light, more specifically the Sagnac Effect [49]. On the other hand, a polarimetric gyroscope is based on a related but distinct phenomenon: the rotation of the plane of polarization of light within a medium due to rotation. The rotation of the polarization is directly proportional to the rotation rate of the device, so the rotation can be measured.

In this section, a rotation sensor is presented, based on the setup shown in Fig. 5.7.

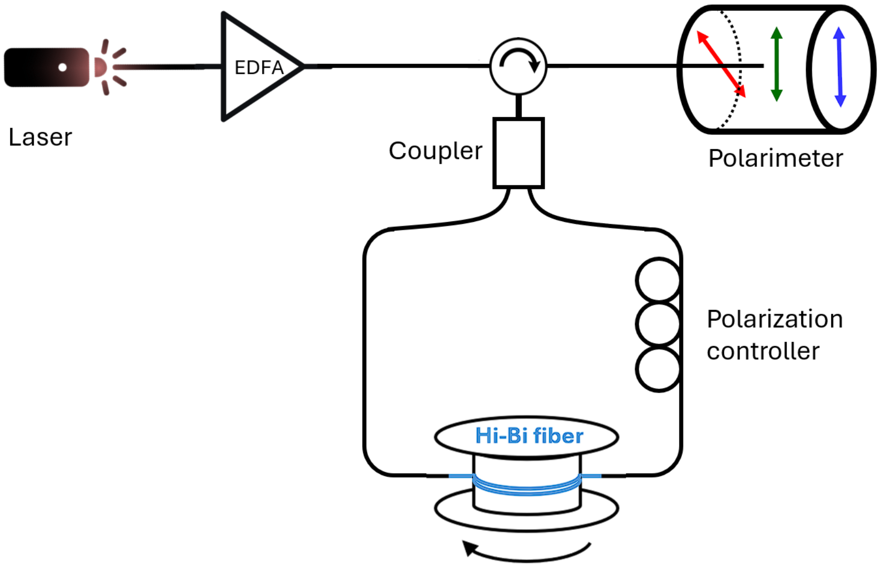

FIGURE 5.7: Setup of the polarimetric rotation sensor using an FLM.

In order to measure rotation, 1 m of hi-bi fiber was curled around a reel and the angle was measured in relation to a support, as shown in Fig. 5.8. This rotation apparatus was then placed in the fiber loop mirror, in order to measure the SOP output depending on the rotation angle.

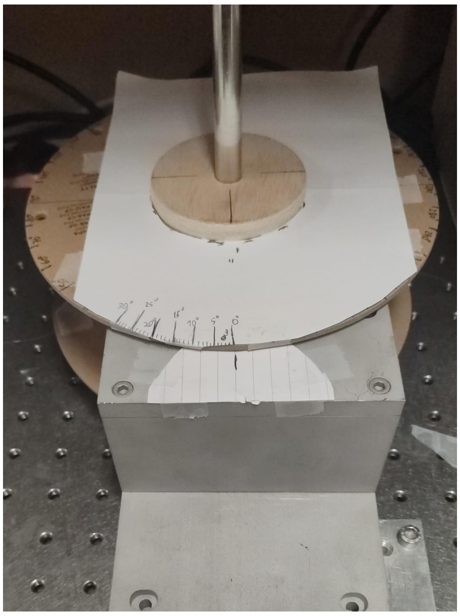

FIGURE 5.8: Apparatus used to apply rotation to the fiber.

Before starting real measurements, the detection limit was determined by measuring the output for two consecutive inputs – 0° and 1° – 10 times each, as is shown in Fig.5.9. The average of the phase obtained for each angle was calculated and the detection limit of the rotation sensor was determined by computing the difference between them.

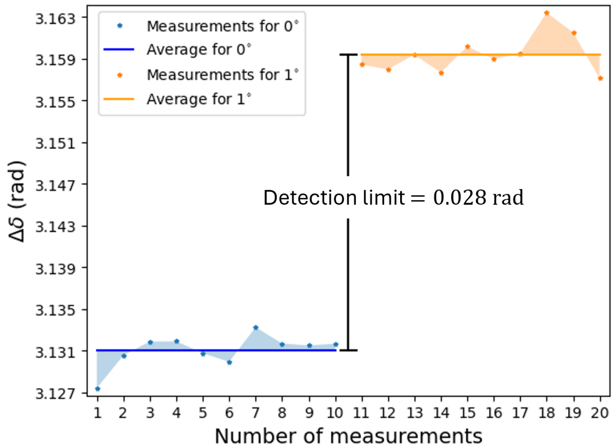

FIGURE 5.9: Light phase as a function of the number of measurements for two different applied rotations: $0°$ and $1°$.

By analyzing the results, it is clear that there is repeatability since the measurements are all close to the average, without significant deviations. In addition to that, the detection limit was determined to be 0.028 rad, while the maximum deviation from the averages was 0.006 rad in both cases. It is also observed that there is a step big enough between $0°$ measurements and $1°$ measurements to conclude that the sensor has enough sensitivity to measure each degree of rotation.

Now that the sensitivity of the sensor was assured, the real measurements can be made. For this, the rotation contraption was used to rotate the fiber loop a total of $30°$ with $1°$ steps. The Stokes parameters, S_2 and S_3, were obtained as a function of the rotation angle, using the polarimeter. Finally, the phase of the light was obtained using Eq. 2.11. Both results are shown in Fig. 5.10.

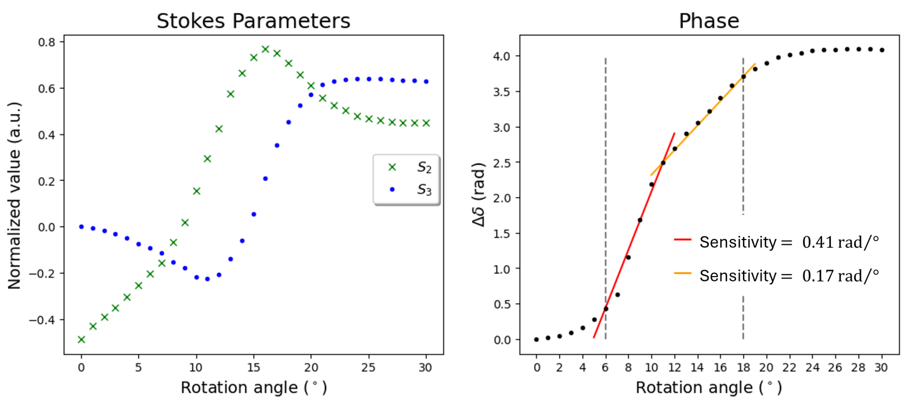

FIGURE 5.10: Stokes parameters (left) and phase (right) as a function of the rotation applied in an FLM.

By examining the phase results, it is apparent that the behavior of the curve is approximately linear in the span of 10° to 20°. Overall, there is clearly a tendency and one can conclude that the rotation of the fiber in the reel affects the SOP and consequently the phase of the light.

The characteristic response of the sensor shows a behavioral trend consistent with the findings reported by Yao et al. [50]. It is important to note, however, that a direct numerical comparison between the datasets is not possible. This limitation arises from a fundamental difference in the measured variables: the referenced work characterizes the phase shift relative to the rotation rate, while the present study analyzes the relationship between phase and the total rotation angle.

All in all, the sensor is capable of measuring rotation, functioning as a gyroscope prototype. In the future, so that this is an accurate rotation sensor, a more precise rotation contraption should be developed, and more degrees of rotation should be included.

5.3. Conclusions

This work successfully investigated and demonstrated one method to enhance the sensitivity of a polarimetric fiber-optic sensor and extended its application to rotation sensing.

The initial strain sensor developed in chapter 4, while satisfactory, presented an opportunity for improvement. It was determined that sensitivity could be increased by employing a high-birefringence fiber and, crucially, by increasing the effective interaction length of the light with the measured parameter. A fiber loop mirror (FLM) was implemented as an effective method to achieve this by enabling a reflective interrogation scheme, effectively doubling the interaction length.

The performance of the FLM-based strain sensor was found to be highly dependent on the initial state of polarization, which dictates the spectral output. Two distinct configurations were tested: one with the output peak aligned at the mid-fringe and another with it at the peak of a fringe. The results were conclusive: the configuration with the peak at the top of the fringe yielded a significantly higher sensitivity (slope of 1.72 ± 0.01 rad $\mu\varepsilon^{-1}$), demonstrating a clear enhancement over the basic sensor setup. In contrast, the mid-fringe configuration resulted in a much lower sensitivity (slope of 0.06 ± 0.01 rad $\mu\varepsilon^{-1}$), even underperforming the original sensor. This demonstrates the importance of optimizing the initial polarization conditions to harness the full potential of an FLM for sensitivity enhancement. Analysis of the Stokes parameters on the Poincaré sphere visually confirmed this vast difference in sensitivity range between the two configurations.

Furthermore, the FLM architecture was adapted to create a proof-of-concept polarimetric rotation sensor. The device demonstrated a clear and measurable response to angular changes, with a determined detection limit of 0.028rad, confirming its ability to resolve rotations as small as 1°. The phase of the light exhibited a perceptible and approximately linear trend with the rotation angle over a specific range, validating the operating principle.

For future work, the rotation sensor's accuracy and range could be improved by developing a more precise rotation mechanism and testing over a wider angular span. In addition to that, in order to measure rotation in all the axis, more degrees of rotation should be added.

6. Conclusions and future work

The aim of this dissertation was to investigate polarization effects in optical fiber systems, both as a source of impairment in amplified communication links and as a sensing mechanism for physical parameters, with a view towards applications in seismic detection. This work successfully developed, characterized, and enhanced a polarimetric sensor, providing valuable insights into its performance, limitations, and potential for real-world applications. To do so, three different studies were performed.

Firstly, a study of the effects of amplification in the polarimeter used was conducted. In this study, the characterization of a commercial EDFA revealed that optical amplification introduces significant polarization-dependent impairments. While the amplifier's gain saturation was not fully reached in the standard configuration, the analysis of Stokes parameters and optical phase demonstrated that the EDFA is a source of Polarization-Dependent Gain (PDG) and, more critically, phase instability. This phase noise was more pronounced at lower input powers and became a dominant factor in a long-haul configuration with 50 km of fiber, where a substantial phase drift was observed. This finding is crucial for the implementation of polarimetric sensing on submarine cables, as it concludes that in-line amplifiers, while necessary for signal transmission, can degrade the very signal (SOP and phase) used for sensing. The optimal operating point was found to be at higher input powers (e.g., -18 dBm in a short fiber and 0-2 dBm in long fiber) to maximize stability, though this is ultimately a trade-off with the risk of saturation.

After, studying the effects of amplification in polarization, a fundamental polarimetric sensor was implemented using a commercial polarimeter to measure Stokes parameters. The system demonstrated a clear and measurable response to three key physical parameters relevant to seismic and environmental sensing:

- Temperature: The sensor detected subtle ambient temperature changes ($\sim 3°C$), confirming its sensitivity despite a non-ideal experimental setup.
- Twist: The sensor exhibited a periodic, sinusoidal response to fiber torsion, validating the underlying principle of twist-induced birefringence. A small calibration shift was identified, attributed to the mechanical contraption used.

- Strain: The sensor showed an excellent linear response to axial strain with a high coefficient of determination. The phase varied linearly with strain, proving the setup's viability for accurate strain measurement.

Chapter 4 confirmed that a simple polarimetric setup in transmission is capable of acting as a multi-parameter sensor with satisfactory accuracy.

Finally, to address the sensitivity limitations of the basic sensor, a high-birefringence Fiber Loop Mirror was implemented. This configuration effectively doubled the interaction length and allowed for reflective interrogation. This setup with the FLM was used for two applications: enhancing strain sensing and employing a rotation sensor. By using the FLM to enhance the sensing capabilities of the strain sensor it was discovered that the performance was critically dependent on the initial SOP, which sets the spectral output. Configuring the output at the peak of an interference fringe yielded a sensitivity (slope of 1.72 ± 0.01 rad $\mu\varepsilon^{-1}$) over ten times greater than the basic strain sensor, while a mid-fringe configuration resulted in significantly lower sensitivity. This highlights that the FLM is not an automatic solution but a powerful tool that requires optimization to unlock its full potential. Acknowledging this, the FLM architecture was successfully adapted to create a proof-of-concept polarimetric rotation sensor (gyroscope). The device demonstrated a measurable response to angular changes, with a determined detection limit of 0.028 rad, capable of resolving rotations as small as 1°. The phase exhibited a perceptible trend with rotation, validating the operating principle.

The findings of this dissertation present several promising avenues for future research and development.

In conclusion, this work has successfully advanced the understanding of polarimetric sensing by characterizing a key noise source (the EDFA), demonstrating robust multi-parameter sensing capabilities, and proving a method to significantly enhance sensitivity. The results strongly support the potential of polarimetric techniques to transform global submarine cable infrastructure into a vast, sensitive network for Earth science and hazard mitigation.

Future work may include developing signal processing techniques to identify the perturbation that occurred and when seismic activity is present. A primary challenge for polarimetric sensors is their inherent cross-sensitivity. In addition to that, the sensor developed should be tested in a more realistic, and controlled environment.

Furthermore, a crucial next step is to transition from a point sensor to a truly distributed sensing system, which is the ultimate goal for seismic monitoring on submarine cables.

Moreover, the FLM setup should be enhanced with an active feedback loop to automatically lock the laser wavelength to the peak of an interference fringe, ensuring maximum sensitivity is consistently maintained regardless of external drift. With this improvement, the rotation sensor could be employed as a working gyroscope by enabling the contraption to measure rotation in all directions.

Ultimately, polarimetric sensing is a promising research area with considerable potential for numerous practical applications, positioning it as a valuable technology for future sensing systems. Despite this promise, the response of the SOP to complex, multi-parameter environmental changes is not yet fully deterministic. To address these uncertainties and enhance the robustness of polarimetric sensors, further fundamental research focused on decoupling the effects of simultaneous perturbations and characterizing SOP behavior under a broader spectrum of operational conditions.

References

[1] [Online]. Available: https://commons.wikimedia.org/w/index.php?curid=2107870 [Cited on pages viii and 4.]

[2] D. Goldstein, *Polarized Light*. CRC Press, 2011. [Cited on page 5.]

[3] R. Talebi, F. Taheri Ghahfarokhi, and D. Vashaee, "Photoinduced tunable birefringence and dichroism in silver nanogratings," *Journal of the Optical Society of America B*, vol. 37, no. 10, p. 2848, Sep. 2020. [Cited on page 7.]

[4] H. Poincare, *Theorie Mathematique de la Lumiere*, 1889. [Cited on page 8.]

[5] A. Fresnel, *The Wave Theory of Light*, 1818. [Cited on page 16.]

[6] G. G. Stokes, "On the change of refrangibility of light," *Philosophical Transactions of the Royal Society of London*, vol. 142, pp. 463–562, 1852. [Online]. Available: http://www.jstor.org/stable/108550 [Cited on page 16.]

[7] I. Kaminow, "Polarization in optical fibers," *IEEE Journal of Quantum Electronics*, vol. 17, no. 1, pp. 15–22, 1981. [Cited on page 16.]

[8] S. Ryu, S. Yamamoto, Y. Namihira, K. Mochizuki, and H. Wakabayashi, "Polarization diversity techniques for the use of coherent optical fiber submarine cable systems," *Journal of Lightwave Technology*, vol. 9, no. 5, pp. 675–682, 1991. [Cited on page 17.]

[9] D. Waddy, P. Lu, L. Chen, and X. Bao, "Fast state of polarization changes in aerial fiber under different climatic conditions," *IEEE Photonics Technology Letters*, vol. 13, no. 9, pp. 1035–1037, 2001. [Cited on page 17.]

[10] L. Palmieri, "Distributed polarimetric measurements for optical fiber sensing," *Optical Fiber Technology*, vol. 19, no. 6, Part B, pp. 720–728, 2013, optical Fiber Sensors. [Online]. Available: https://www.sciencedirect.com/science/article/pii/S1068520013000953 [Cited on page 17.]

[11] Z. Zhan, M. Cantono, V. Kamalov, A. Mecozzi, R. Müller, S. Yin, and J. C. Castellanos, "Optical polarization–based seismic and water wave sensing on transoceanic cables," *Science*, vol. 371, no. 6532, pp. 931–936, 2021. [Online].

Available: https://www.science.org/doi/abs/10.1126/science.abe6648 [Cited on page 18.]

[12] A. Mecozzi, M. Cantono, J. C. Castellanos, V. Kamalov, R. R. Muller, and Z. Zhan, "Polarization sensing using submarine optical cables," *Optica*, 2021. [Online]. Available: https://api.semanticscholar.org/CorpusID:235506853 [Cited on page 18.]

[13] A. Mecozzi, "Sensing with submarine optical cables," *APL Photonics*, vol. 9, no. 7, p. 070902, 07 2024. [Online]. Available: https://doi.org/10.1063/5.0210825 [Cited on page 18.]

[14] L. Costa, S. Varughese, and P. Mertz, "Localization of seismic waves with submarine fiber optics using polarization-only measurements," *Commun Eng*, vol. 2, no. 86, 2023. [Cited on page 18.]

[15] M. Mazur, J. C. Castellanos, R. Ryf, E. Börjeson, T. Chodkiewicz, V. Kamalov, S. Yin, N. K. Fontaine, H. Chen, L. Dallachiesa, S. Corteselli, P. Copping, J. Gripp, A. Mortelette, B. Kowalski, R. Dellinger, D. T. Neilson, and P. Larsson-Edefors, "Transoceanic phase and polarization fiber sensing using real-time coherent transceiver," in *2022 Optical Fiber Communications Conference and Exhibition (OFC)*, 2022, pp. 1–3. [Cited on page 18.]

[16] M. Mazur, D. Wallberg, L. Dallachiesa, E. Börjeson, R. Ryf, M. Bergroth, B. Josefsson, N. K. Fontaine, H. Chen, D. T. Neilson, J. Schröder, P. Larsson-Edefors, and M. Karlsson, "Real-time monitoring of cable break in a live network using a coherent transceiver prototype," in *2024 Optical Fiber Communications Conference and Exhibition (OFC)*, 2024, pp. 1–3. [Cited on page 19.]

[17] R. Mears, L. Reekie, S. Poole, and D. Payne, "Low-threshold tunable CW and Q-switched fibre laser operating at 1.55 µm," *Electronics Letters*, vol. 22, pp. 159–160, 1986. [Online]. Available: https://digital-library.theiet.org/doi/abs/10.1049/el:19860111 [Cited on page 20.]

[18] R. Mears, L. Reekie, I. Jauncey, and D. Payne, "Low-noise erbium-doped fibre amplifier operating at 1.54 µm," *Electronics Letters*, vol. 23, pp. 1026–1028, 1987. [Online]. Available: https://digital-library.theiet.org/doi/abs/10.1049/el:19870719 [Cited on page 20.]

[19] Hamida, C. San, Mahdi, M. Adzir, S. Harun, Wadi, S. Khan, A.-K. Zaidan, A. Ahmad, and H, "Review of erbium-doped fiber amplifier," vol. 6, 09 2011. [Cited on page 20.]

[20] R. Mears and S. Baker, "Erbium fibre amplifiers and lasers," *Optical and Quantum Electronics*, vol. 24, no. 5, pp. 517–538, 5 1992. [Cited on page 20.]

[21] T. Li, J. Cui, C. Diao, X. Gong, and S. Jian, "Testing polarization-dependent gain of erbium-doped fiber amplifiers," *Proceedings of SPIE - The International Society for Optical Engineering*, vol. 5279, 04 2004. [Cited on page 20.]

[22] V. Mazurczyk and J. Zyskind, "Polarization dependent gain in erbium doped-fiber amplifiers," *IEEE Photonics Technology Letters*, vol. 6, no. 5, pp. 616–618, 1994. [Cited on page 20.]

[23] D. Peterson, B. Ward, K. Rochford, P. Leo, and G. Simer, "Polarization mode dispersion compensator field trial and field fiber characterization," *Optics Express*, vol. 10, pp. 614–621, 07 2002. [Cited on page 20.]

[24] J. P. Gordon and H. Kogelnik, "Pmd fundamentals: Polarization mode dispersion in optical fibers," *Proceedings of the National Academy of Sciences*, vol. 97, no. 9, pp. 4541–4550, 2000. [Online]. Available: https://www.pnas.org/doi/abs/10.1073/pnas.97.9.4541 [Cited on page 20.]

[25] M. Karlsson, J. Brentel, and P. A. Andrekson, "Long-term measurement of pmd and polarization drift in installed fibers," *Journal of Lightwave Technology*, vol. 18, no. 7, pp. 941–951, 2000. [Cited on page 20.]

[26] T. Woliński, P. Lesiak, and A. Domański, "Polarimetric optical fiber sensors of a new generation for industrial applications," *BULLETIN OF THE POLISH ACADEMY OF SCIENCES TECHNICAL SCIENCES*, vol. 56, 06 2008. [Cited on page 33.]

[27] R. K. Gangwar, S. Kumari, A. K. Pathak, S. D. Gutlapalli, and M. C. Meena, "Optical fiber based temperature sensors: A review," *Optics*, vol. 4, no. 1, pp. 171–197, 2023. [Online]. Available: https://www.mdpi.com/2673-3269/4/1/13 [Cited on page 33.]

[28] M. Shribak, "Optical polarimetric temperature sensor," *Proc SPIE*, pp. 260–265, 08 1998. [Cited on page 34.]

[29] V. Budinski and D. Donlagic, "Fiber-optic sensors for measurements of torsion, twist and rotation: A review," *Sensors*, vol. 17, no. 3, p. 443, 2 2017. [Cited on page 35.]

[30] Y. Wang, L. Liang, Y. Yuan, G. Xu, and F. Liu, "A two fiber bragg gratings sensing system to monitor the torque of rotating shaft," *Sensors*, vol. 16, no. 1, p. 138, 1 2016. [Cited on page 35.]

[31] Y. Kong, X. Shu, and Z. Xu, "A novel in-fiber helical long period grating with small period inscribed by femtosecond laser for twist sensing with comprehensive performance," *IEEE Transactions on Instrumentation and Measurement*, vol. 73, pp. 1–15, 2024. [Cited on page 35.]

[32] J. Fu, J. Guan, S. Ding, Y. Chen, P. Huang, Z. Wei, C. Tan, F. Wang, and H. Meng, "Pmf based sagnac interferometric sensor for simultaneous measurement of strain, temperature, and torsion," *Optics Communications*, vol. 573, p. 130883, 2024. [Online]. Available: https://www.sciencedirect.com/science/article/pii/S0030401824006205 [Cited on page 35.]

[33] J. Yang, W. Zhang, Y. Zhang, X. Kang, Y. Zhang, L. Kong, T. Yan, and L. Chen, "Temperature-insensitive polarimetric torsion sensor based on a pair of angularly cascaded lpfgs," *Optical Fiber Technology*, vol. 46, pp. 11–14, 2018. [Online]. Available: https://www.sciencedirect.com/science/article/pii/S1068520018304140 [Cited on page 35.]

[34] D. Lesnik and D. Donlagic, "In-line, fiber-optic polarimetric twist/torsion sensor," *Opt. Lett.*, vol. 38, no. 9, pp. 1494–1496, May 2013. [Online]. Available: https://opg.optica.org/ol/abstract.cfm?URI=ol-38-9-1494 [Cited on page 35.]

[35] S. Yang, Q. Zhang, X. Li, Q. Wang, and Y. Li, "Optical fiber strain sensor with high and tunable sensitivity," *Review of Scientific Instruments*, vol. 94, no. 11, p. 115003, 11 2023. [Online]. Available: https://doi.org/10.1063/5.0154895 [Cited on page 37.]

[36] Y. Wang, X. Qiao, H. Yang, D. Su, L. Li, and T. Guo, "Sensitivity-improved strain sensor over a large range of temperatures using an etched and regenerated fiber bragg grating," *Sensors*, vol. 14, no. 10, pp. 18 575–18 582, 2014. [Online]. Available: https://www.mdpi.com/1424-8220/14/10/18575 [Cited on page 37.]

[37] Y. Wei, H. Xiang, C. Liu, J. Kang, Y. Tang, P. Ren, X. Wang, and Z. Liu, "Highly sensitive threaded lpfg strain sensor," *Measurement*, vol. 242, p. 116012, 2025. [Online]. Available: https://www.sciencedirect.com/science/article/pii/S0263224124018979 [Cited on page 37.]

[38] X. Dong, Z. Luo, H. Du, X. Sun, K. Yin, and J. Duan, "Highly sensitive strain sensor based on a novel mach–zehnder mode interferometer with tcf-pcf-tcf structure," *Optics and Lasers in Engineering*, vol. 116, pp. 26–31, 2019. [Online].

Available: https://www.sciencedirect.com/science/article/pii/S0143816618302513 [Cited on page 37.]

[39] C. R. Liao, D. N. Wang, and Y. Wang, "Microfiber in-line mach–zehnder interferometer for strain sensing," *Opt. Lett.*, vol. 38, no. 5, pp. 757–759, Mar 2013. [Online]. Available: https://opg.optica.org/ol/abstract.cfm?URI=ol-38-5-757 [Cited on page 37.]

[40] M. Yan, X. Tan, S. Mahjoubi, and Y. Bao, "Strain transfer effect on measurements with distributed fiber optic sensors," *Automation in Construction*, vol. 139, p. 104262, 2022. [Online]. Available: https://www.sciencedirect.com/science/article/pii/S0926580522001352 [Cited on page 37.]

[41] S. Sumriddetchkajorn and N. A. Riza, "Fiber-connectorized multiwavelength 2×2 switch structure using a fiber loop mirror," *Optics Communications*, vol. 175, no. 1, pp. 89–95, 2000. [Online]. Available: https://www.sciencedirect.com/science/article/pii/S0030401899007439 [Cited on page 40.]

[42] A. Siahlo, L. Oxenlwe, K. Berg, A. Clausen, P. Andersen, C. Peucheret, A. Tersigni, P. Jeppesen, K. Hansen, and J. Folkenberg, "A high-speed demultiplexer based on a nonlinear optical loop mirror with a photonic crystal fiber," *IEEE Photonics Technology Letters*, vol. 15, no. 8, pp. 1147–1149, 2003. [Cited on page 40.]

[43] P. Robalinho, B. Soares, A. Lobo Ribeiro, S. Silva, and O. Frazão, "Fiber loop mirror based on optical fiber circulator for sensing applications," *Sensors*, vol. 23, no. 2, p. 618, 1 2023. [Cited on page 40.]

[44] O. Frazão, J. M. T. Baptista, and J. L. Santos, "Recent advances in high-birefringence fiber loop mirror sensors," *Sensors*, vol. 7, no. 11, pp. 2970–2983, 2007. [Online]. Available: https://www.mdpi.com/1424-8220/7/11/2970 [Cited on page 40.]

[45] 9 2025. [Cited on page 44.]

[46] V. Passaro, A. Cuccovillo, L. Vaiani, M. De Carlo, and C. Campanella, "Gyroscope technology and applications: A review in the industrial perspective," *Sensors*, vol. 17, no. 10, p. 2284, 10 2017. [Cited on page 44.]

[47] Z. Chen, K. Yan, X. Wang, R. Li, A. Zhang, X. Wang, Y. Wang, P. Gao, H. Li, C. Wang, J. Zhang, M. Liu, and Q. Lu, "Mems gyroscopes in different

operation modes: A review," *Measurement*, vol. 249, p. 116996, 2025. [Online]. Available: https://www.sciencedirect.com/science/article/pii/S0263224125003550 [Cited on page 44.]

[48] H. Guo, H. Liu, M. Lei, M. Tan, and Z. Song, "Research progress of integrated optical gyroscope," *Chinese Optics Letters*, vol. 22, no. 11, p. 031302, 3 2024. [Online]. Available: https://www.researching.cn/articles/OJ8e7cb5eab35a9d2f [Cited on page 44.]

[49] A. A. Untilov, E. V. Dranitsyna, and D. A. Egorov, "Current state and development prospects of fiber-optic gyroscopes," in *2023 30th Saint Petersburg International Conference on Integrated Navigation Systems (ICINS)*, 2023, pp. 1–4. [Cited on page 44.]

[50] X. S. Yao, H. Xuan, X. Chen, H. Zou, X. Liu, and X. Zhao, "Polarimetry fiber optic gyroscope," *Opt. Express*, vol. 27, no. 14, pp. 19 984–19 995, Jul 2019. [Online]. Available: https://opg.optica.org/oe/abstract.cfm?URI=oe-27-14-19984 [Cited on page 47.]

[51] [Online]. Available: https://www.thorlabs.com/newgrouppage9.cfm?objectgroup_id=6673 [Cited on pages ix and 58.]

A. Beam Splitter

This appendix presents a study of a polarimetric sensor based on a beam splitter configuration. The experimental setup, illustrated in Fig. A.1, is designed to reproduce the key features of communication cables through the emulation of an optical transceiver. This involves splitting the light propagating through the cable into two orthogonally polarized components (x and y), thereby replicating the functionality of transceivers found in submarine cables.

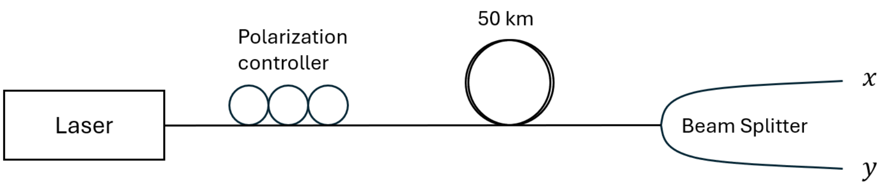

FIGURE A.1: Setup used to reproduce the key features of communication cables.

To characterize the beam splitter and verify the orthogonality of its two output states, torsion* was applied to the fiber. Since the beam splitter separates the input light into horizontal (x, port 2) and vertical (y, port 1) polarization components, as shown in Fig. A.2, the SOP at each output remains fixed. Therefore, any external perturbation primarily affects the signal intensity.

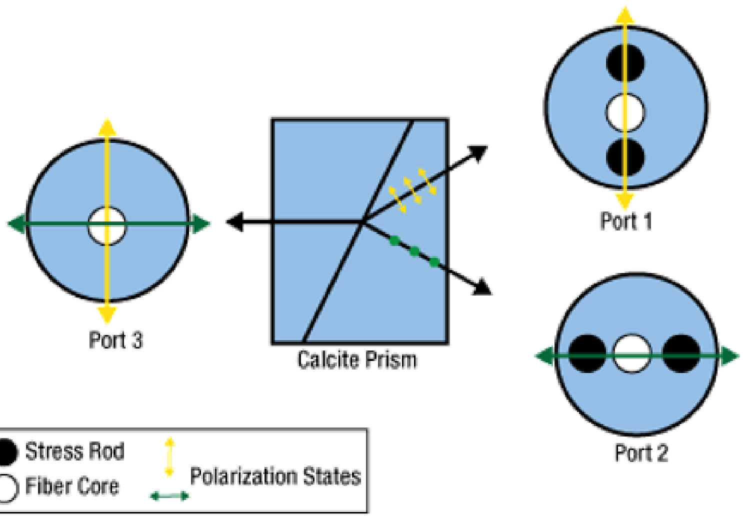

FIGURE A.2: Polarization Beam Combiner/Splitter, 2 PM Ports [51].

*The configuration did not have enough sensitivity to detect strain.

The orthogonal behavior of the beam splitter was characterized by measuring the power at both outputs. This measurement was performed for the two ports x and y, as shown in Fig. A.3.

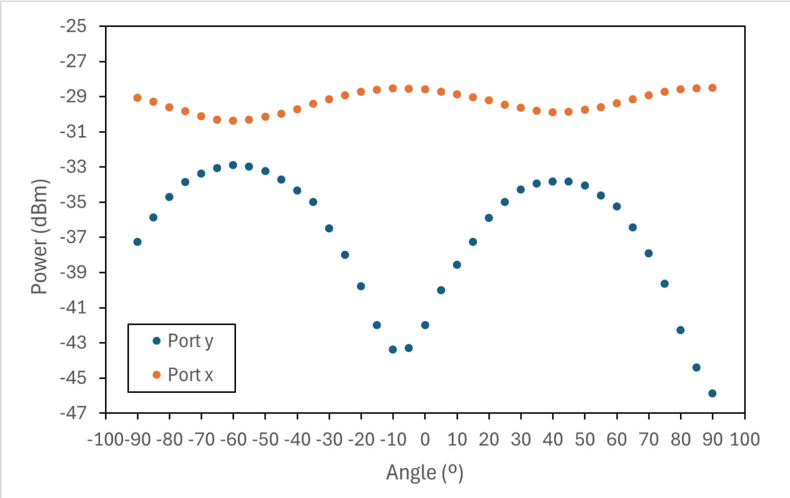

FIGURE A.3: Power of the two ports x and y as a function of the angle of torsion.

The results seem to indicate that the two ports have completely different behaviors. However, with a more thorough analysis it is noticeable that there is a opposite relation between the x and y signals. It is also important to note that the y signal has a bigger range of operation.

In order to directly compare and test the orthogonality of the two outputs, the results obtained were linearized and normalized, as is illustrated in Fig. A.4.

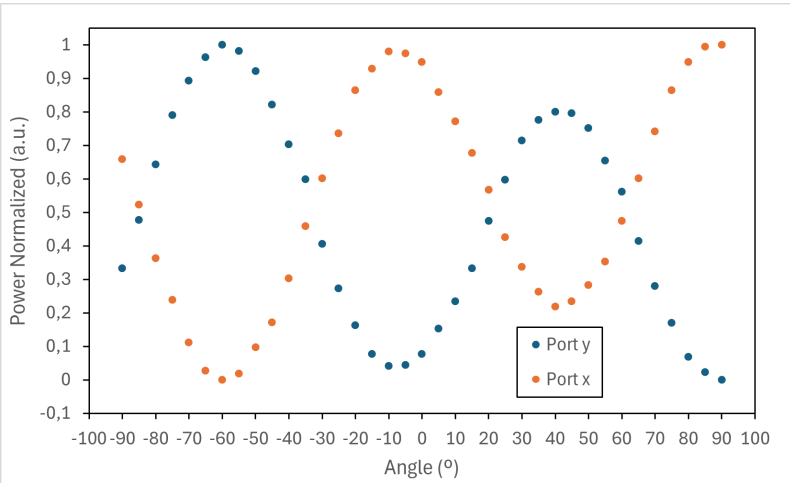

FIGURE A.4: Power of the two ports x and y normalized as a function of the angle of torsion.

The results demonstrate that the sensor is capable of accurately sensing twist, since there is a sinusoidal behavior. In addition to that a distinct opposite relationship between the x and y signals is evident.

It is concluded that the observed anti-phase behavior between the two ports proves their orthogonality. Additionally, the sensor has a better response when the SOP is vertical.